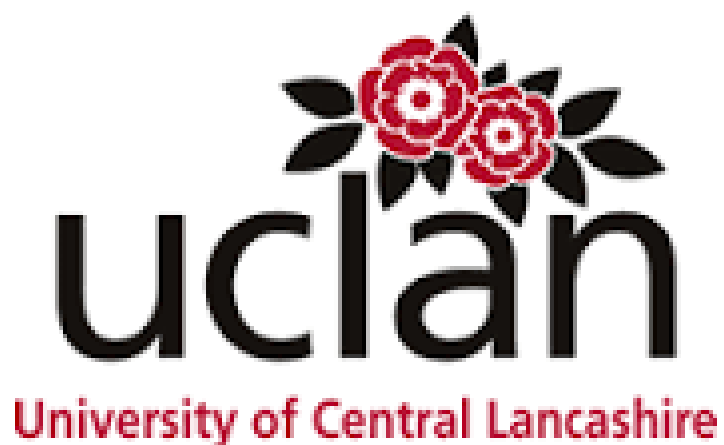


# Carbogenic Nanoparticles for Biomedical Applications

*Jordan Wilkinson*

*September 2017*



*Dissertation for full-time MSc Chemistry degree*

*Supervisor: Dr. Antonios Kelarakis*

*School of Physical Sciences and Computing*

## Declaration of Work

I declare that this is my own work, with all information taken from references identified and acknowledged at the end of this thesis.

Date: **02/10/2017**

Signed: 

Word count: 13,218

## Acknowledgements

Many thanks to Dr. Antonios Kelarakis and Diogo Ferdandes for their guidance and support in completing this study.

I would also like to thank my father for his constant support, allowing me to continue through difficult times.

## Table of Contents

Declaration of Work.....	1
Acknowledgements.....	2
Glossary.....	5
List of Figures .....	6
List of Tables.....	7
Abstract.....	8
1. Introduction .....	9
1.1 Carbogenic Nanoparticles as Photoluminescent Materials .....	9
1.1.1 Formation Mechanism and Properties of Carbogenic Nanoparticles.....	10
1.1.2 Fluorescence Mechanism of Carbogenic Nanoparticles .....	12
1.1.3 Bioimaging with Carbogenic Nanoparticles .....	13
1.1.4 Toxicity of Carbogenic Nanoparticles.....	15
1.1.5 Carbogenic Nanoparticles for Drug Delivery.....	16
1.2 Polymeric Prodrugs as a Model Drug Delivery System .....	17
1.2.1 Structure of Polymeric Prodrugs.....	18
1.2.2 Advantages of Polymeric Prodrugs .....	20
1.3 Hydrogels as a Drug Delivery System.....	22
1.3.1 Types of Hydrogels and Categorisation .....	23
1.3.2 Advantages of Hydrogels .....	24
1.3.4 Fluorescent Dyes in Hydrogels.....	27
1.4 Pluronic® Surfactants for Preparing Hydrogels.....	28
1.4.1 Self-Assembly in Water .....	29
1.4.2 Drug Solubilisation and Delivery .....	30
1.5 JEFFAMINES® for Functionalisation of C-dots.....	32
1.6 Paracetamol for Drug Release Profiles .....	33
1.7 Ibuprofen for Drug Release Profiles.....	34
1.8 Research Project Objectives.....	35
.....	36
.....	36
2. Materials and Methodology.....	37
2.1 Materials .....	37
2.2 Methodology.....	37
2.2.1 Carbogenic Nanoparticles Synthesis (aC-dots) .....	37
2.2.2 Functionalisation with JEFFAMINES® .....	38

2.2.3 Encapsulation of C-dots in Hydrogels .....	39
2.2.4 Gel Phase Behaviours .....	39
2.2.5 Fluorescence Behaviours .....	40
2.2.6 Pluronic® Hydrogel Preparation and Drug Loading .....	40
2.2.7 <i>In Vitro</i> Drug Release Studies .....	43
3. Results and Discussion .....	45
3.1 Characterization of Carbogenic Nanoparticles .....	45
3.2 Fluorescence Properties of Carbogenic Nanoparticles .....	47
3.2.1 Fluorescence Spectra of Carbogenic Nanoparticles.....	49
3.2.2 Fluorescence Microscopy Images .....	54
3.3 Gel Phase Behaviour .....	56
3.4 Drug Release Studies.....	58
3.4.1 Ibuprofen Calibration Curve.....	58
3.4.2 Release Profiles without C-dots .....	59
3.4.3 Release Profiles with C-dots.....	60
3.4.4 Release Profiles of Paracetamol and Ibuprofen Compared .....	63
4. Conclusion .....	64
References.....	66

## Glossary

C-dots	Carbogenic Nanoparticles
CMC	Critical Micelle Concentration
CMT	Critical Micelle Temperature
D-230 (JD-230)	JEFFAMINE® D-230
D-400 (JD-400)	JEFFAMINE® D-400
DOX	Doxorubicin
DTX	Docetaxel
IBU	Ibuprofen
mPEG	Methoxy-poly(ethylene glycol)
MWCO	Molecular Weight Cut-off
MW	Molecular weight
P-123	Pluronic® P-123
PBS	Phosphate Buffer Solution
PCL	Paracetamol
PEG	Poly(ethylene glycol)
PEO	Poly(ethylene oxide)
PPO	Poly(propylene oxide)
PTX	Paclitaxel
UV	Ultraviolet
UV-vis	Ultraviolet-Visible
$\lambda_{\text{ex}}$	Excitation Wavelength

## List of Figures

<b>Figure 1.1.</b> <i>The various structures of C-dots that were used in the attempt to devise a fluorescence mechanism.....</i>	<i>12</i>
<b>Figure 1.2.</b> <i>In vivo fluorescence images upon the injection of C-dots subcutaneously into live mice, with various wavelength excitations. In addition, the fluorescence intensities at different excitation wavelengths are shown in a graph.....</i>	<i>14</i>
<b>Figure 1.3.</b> <i>Cell viabilities after exposure to various concentrations of three types of C-dots.....</i>	<i>15</i>
<b>Figure 1.4.</b> <i>Ringsdorf model of a polymeric prodrug.....</i>	<i>19</i>
<b>Figure 1.5.</b> <i>HA/Pluronic® hydrogels slightly cross-linked 3-D network formation and their sol-gel transition characteristics.....</i>	<i>23</i>
<b>Figure 1.6.</b> <i>Sol-gel phase diagram example of a triblock co-polymer in aqueous solution. The sol-gel transitions are shown as the circles, and the squares represent the temperatures at which the gel becomes turbid, acquired from references.....</i>	<i>25</i>
<b>Figure 1.7.</b> <i>Formation of micelles as an overall mechanism for polymers. In triblock copolymers there will be two hydrophobic tails representing the PEO in PEO-PPO-PEO.....</i>	<i>29</i>
<b>Figure 1.8.</b> <i>Drug loading of a typical micelle ‘unimer’ using a hydrophobic drug. This is done via self-assembly.....</i>	<i>31</i>
<b>Figure 1.9.</b> <i>D Series JEFFAMINE® representative structure.....</i>	<i>32</i>
<b>Figure 1.10.</b> <i>The chemical structure of PCL (para-acetylamino phenol).....</i>	<i>33</i>
<b>Figure 1.11.</b> <i>The chemical structure of Ibuprofen (4-isobutyl-<math>\alpha</math>-methylphenylacetic acid).....</i>	<i>34</i>
<b>Fig. 1.12.</b> <i>Schematic drawing illustrating the experimental process in this research project.....</i>	<i>36</i>
<b>Fig 2.1.</b> <i>Ibuprofen calibration curve using various concentrations of IBU (0.01, 0.03, 0.05, 0.07, 0.09, 0.1, 0.3, 0.5, 0.7, 0.9) in a phosphate buffer solution at pH 7.4. Absorbances taken at 263 nm as determined by UV-vis spectra in conjunction with literature.....</i>	<i>44</i>
<b>Fig 2.2.</b> <i>Paracetamol calibration curve using various concentrations of PCL (0.01, 0.03, 0.05, 0.07, 0.09, 0.1, 0.3, 0.5, 0.7, 0.9) in a phosphate buffer solution. Absorbance taken at 243 nm as determined from UV spectra in conjunction with literature.....</i>	<i>44</i>
<b>Figure 3.1.</b> <i>Tunnelling Electron Microscope images of the C-dots that were synthesised using the protocol in this project, and size histograms. Acquired from Reference.....</i>	<i>45</i>
<b>Figure 3.2.</b> <i>FTIR spectra to show the presence of imide and amide functional groups on the surface of the C-dots. Acquired from reference.....</i>	<i>46</i>
<b>Figure 3.3.</b> <i>Raman spectrum of C-dots after being exposed to a temperature of 300°C. Acquired from reference.....</i>	<i>46</i>

<b>Figure 3.4.</b> Images of the fluorescence characteristics of 32.5% w/t P-123 hydrogel samples with aC-dots, and dilute solutions of aC-dots, JD-230 C-dots and JD-400 C-dots respectively from left to right. The pluronic gel was made at a concentration of 0.103 mg/ml and each dilute solution was maintained at 0.05 mg/ml.....	47
<b>Figure 3.5.</b> Solid-like state fluorescence spectra of Pluronic® P-123 32.5% w/t hydrogel with 0.103 mg/ml aC-dots at excitation wavelengths 300, 340, 380, 420, 460 and 500 nm.....	49
<b>Figure 3.6.</b> Liquid state fluorescence spectra of a 0.05 mg/ml solution of aC-dots with water at excitation wavelengths 320, 350, 380, 410, 440, 470 and 500 nm.....	51
<b>Figure 3.7.</b> Liquid state fluorescence spectra of a 0.05 mg/ml solution of JD-230 C-dots and water at excitation wavelengths 320, 350, 380, 410, 440, 470 and 500 nm.....	51
<b>Figure 3.8.</b> Liquid state fluorescence spectra of a 0.05 mg/ml solution of JD-400 C-dots and water at excitation wavelengths 320, 350, 380, 410, 440, 470 and 500 nm.....	53
<b>Figure 3.9.</b> Fluorescence microscopy images of sample vials with water, aC-dots, JD-230 C-dots and JD-400 C-dots (top to bottom respectively) when exposed to light at wavelengths 350, 395 and 590 nm using a fluorescence microscope with band-pass filters.....	55
<b>Fig 3.10.</b> Gel phase behaviours of 32.5% w/t P-123 hydrogels with the presence of various types of C-dots and without any C-dots, shown in the form of a histogram.....	57
<b>Figure 3.11.</b> Ibuprofen calibration curve via UV analysis of various concentrations (0.01, 0.03, 0.05, 0.07, 0.09, 0.1, 0.3, 0.5, 0.7, 0.9 mg/ml) of IBU in a pH 7.4 buffer solution.....	58
<b>Figure 3.12.</b> Release profiles of Ibuprofen from Pluronic® P-123 hydrogels against a phosphate buffer solution (pH 7.4) at room temperature, without the presence of any C-dots.....	59
<b>Figure 3.13.</b> Release profiles of Ibuprofen from Pluronic® P-123 hydrogels against a phosphate buffer solution (pH 7.4) at room temperature. The squares represent the gel without the presence of any C-dots is, and the circles, diamonds and triangles represent the gels with JD-230 C-dots, JD-400 C-dots and aC-dots respectively.....	60
<b>Fig 3.14.</b> In vitro release profiles of PCL and ibuprofen in P-123 hydrogel with the presence of aC-dots against a phosphate buffer solution (pH 7.4).....	63

## List of Tables

<b>Table 2.1.</b> The masses used to synthesise Pluronic® hydrogels with varying C-dots and drugs...42
--

## Abstract

In this study we focus on the incorporation of an emerging class of non-toxic and photoluminescent materials, namely carbogenic nanoparticles or C-dots, to Pluronic® hydrogels. The role of C-dots in those systems is dual; first C-dots can impart significant photoluminescent properties absolutely desirable for bioimaging purposes. Second, C-dots are expected to be able to offer a further degree of control on the drug release profile of the system. The C-dots were synthesised from citric acid monohydrate and ethanolamine using a pyrolysis method at 300°C and were functionalised with JEFFAMINES® D-230 and D-400. This study shows that C-dots encapsulated in hydrogels exhibit high levels of fluorescence in analogy with the well-established behaviour of the dilute aqueous dispersions. The release profiles of ibuprofen from the Pluronic® gel suggest that incorporation of C-dots significantly modifies the diffusion kinetics in a manner that depends upon the surface functionalities of the nanoparticles. Release profiles of paracetamol from the Pluronic® gel were also observed, and compared with that of ibuprofen. The faster kinetics observed for C-dot containing hydrogels indicate that addition of nanoparticles effectively releases the close packing constrains of the gel.

# 1. Introduction

## 1.1 Carbogenic Nanoparticles as Photoluminescent Materials

Fluorescent materials are currently in enormous demand for many areas and disciplines, due to their ability to be used in chemical sensing, drug delivery and bioimaging just to name a few<sup>1-3</sup>. The main obstacles for the development of current chemical sensors are the complex process of operation and low levels of sensitivity. These requirements can be easily fulfilled with techniques that involve fluorescent materials, making fluorescent based sensors a candidate with the most potential for chemical sensing<sup>4</sup>. A potential use for these chemical sensors is to detect explosives and hazardous chemicals, and with recent acts of terrorism, this prospect will be in the spotlight<sup>5, 6</sup>. In 2004, a new prodigy of sensors had been discovered in the form of carbogenic nanoparticles, alternatively known as carbon dots (C-dots) and recognised as a new category of nano-emitters that are photoluminescent. They have become the primary focus with regards to fluorescence imaging due to being tuneable and already having desirable characteristics<sup>7</sup>.

Currently, the amount of medicines involving nanotechnology is climbing, set to spread exponentially<sup>8</sup>. These C-dots are investigated extensively in a vast range of technological applications, with the interest in the C-dots being because of their fluorescent properties, economic tuneability, versatility and preparation<sup>1-3</sup>. In addition, the clear advantages of these C-dots in various uses with regards to their outstanding characteristics involve a high cell permeability, photostability, chemical stability, great water dispersability, low toxicity, multicolour emission based on excitation wavelength, and modifiable easily<sup>9</sup>. The surface of the C-dots are also easy to functionalise and as a result can be synthesised to have high solubility in formulations that are water based<sup>10</sup>. Scientists must consider the brightness and photostability

of these luminescent quasi-spherical nanoparticles, especially with them being highly resistant to photobleaching – resulting in a high quantum yield<sup>9</sup>.

A study lead by Wen Sun *et al.* discovered that the fluorescence of the C-dots was stable when exposed to variations in environmental conditions such as UV irradiation, pH and temperature. These C-Dots were also observed to be highly selective and sensitive towards ferric ions<sup>11</sup>.

The ability to disperse and emission intensity of the C-dots is affected significantly depending on the environment the C-dots are exposed to. A carbogenic core in combination with surface groups is what causes the characteristic fluorescent properties of C-dots. These C-dots have an increased resistance against photobleaching, a very low toxicity and minimal invasiveness, which gives them dramatic advantages over quantum dots and polyaromatic dyes. The structure of the carbogenic core can vary from highly graphitic to completely amorphous, depending on the starting materials and the synthetic method used<sup>1-3</sup>. The fluorescent nature of the C-dots allows the interactions involving these nanoparticles to be visualized, and shows fluid longitudinal tracking at an individual cell level, at target organs/tissues and of the whole animal<sup>12</sup>.

### 1.1.1 Formation Mechanism and Properties of Carbogenic Nanoparticles

Usually, carbogenic nanoparticles can be synthesised in two ways, these methods are known as the bottom- up pathway and the top-down pathway. C-dots are synthesised via the bottom-up pathway from raw materials using hydrothermal, oxidation, supported synthesis, microwave, ultrasonic and combustion methods<sup>9</sup>. However, the C-dots formed via the top-down pathway are synthesised through the breaking down of bulk materials, using methods such as arc discharge, plasma treatment, laser ablation and electrochemical exfoliation<sup>9</sup>.

More specifically, the formation mechanism of these C-dots was observed and studied via the pyrolysis of ethanolamine (EA)-citric acid (CA) precursor at varying temperatures. The results show that the fluorescence levels of the C-dots directly correlate to the conditions that they were synthesised in. At high pyrolysis temperatures, the carbogenic core starts to form, but at low temperatures the molecular fluorophores are dominant. The fluorescence becomes solely responsible from the carbogenic cores at very high temperatures, exclusively from the cores at 400° and mostly at 300°C. At lower temperatures (approx. 230°C), the carbogenic core has only just started to form and the fluorescence emission levels are shared with the molecular fluorophores. At 180°C, a high quantum yield via the dehydration of EA-CA can be seen, and the pyrolysis at this temperature resulted in a C-dot molecular precursor with a very intense fluorescence, but without any fluorescence from the carbogenic cores because they had not formed at this temperature<sup>8</sup>.

The C-dots are made up of amorphous nanocrystalline cores with turbostratic carbon shells that can be graphitic or amorphous<sup>9, 13, 14</sup>. They are mainly synthesised of oxygen, hydrogen and carbon atoms with varying ratios between different types of C-dots. There have been investigations involving heteroatoms, attempting to create freedom for extra functions and change the position band of the C-dots conduction to modify the HOMO-LUMO gap. Involving nitrogen could dramatically improve the quantum yield, meanwhile involving sulphur with the C-dots resulted in a wide band gap<sup>15-23</sup>. Furthermore, a surface passivation method devised by Sun's group was utilized to result in an improvement of the quantum yield of C-dots. The most fluorescent C-dots showed a quantum yield of 60%, as a result of modifying the non-fluorescent C-dots with diamine-terminated poly(ethylene glycol) (PEG1500N). Separation was done using an aqueous gel column<sup>24</sup>.

### 1.1.2 Fluorescence Mechanism of Carbogenic Nanoparticles

Typically, fluorescence can be described as the absorption of electromagnetic radiation, usually light, and then the emission of light that is generally of a longer wavelength, which therefore has a lower energy level than that the light being absorbed. However, the behaviour that fascinates most scientists comes when fluorescence materials are exposed to light in the UV region of the spectrum. When a fluorescent substance absorbs UV light, which is invisible to the human eye, it emits visible light in an array of colours. This light emission then immediately dissipates upon the removal of the UV light source.

However, the mechanism that causes the fluorescence these C-dots is under speculation according to researchers. Since there is such a wide variety of C-dots, different mechanisms must be explored using various types of nanoparticles<sup>12</sup>, illustrated below (**Fig. 1.1**).

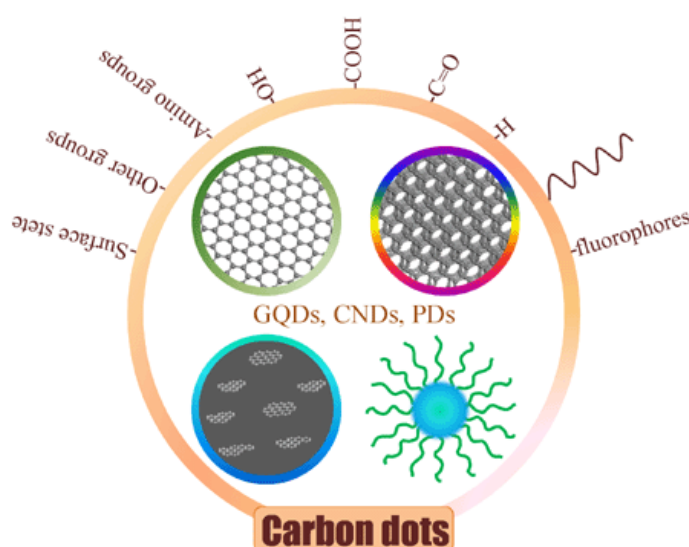


**Fig. 1.1.** The various structures of C-dots that were used in the attempt to devise a fluorescence mechanism<sup>12</sup>.

First, graphene-quantum dots (GQDs) have been used as an example of a fluorescent nanoparticle and used to derive a potential overall mechanism. It is thought that the fluorescence in these GQDs could be caused by several things. Reasons for their fluorescence can be due to: (1) defects and surfaces states<sup>25</sup>, (2) surface passivation<sup>26</sup>, (3) surface groups<sup>27</sup>,

(4) different sized nanoparticles optical selection<sup>28</sup>, (5) fluorophores with different degrees of  $\pi$  conjugation<sup>29, 30</sup>, or (6) the radiative recombination in pairs of electron-holes in  $sp^2$  clusters<sup>31</sup>.

Second, experiments carried out by Kang *et al.* involving carbon nanodots (CNDs) showed that fluorescence properties were affected by the size of the nanoparticles. Emission wavelengths started at UV and changed through to infrared when the CNDs were small through to relatively large respectively. Further investigation showed that the strong emission levels coming from the C-dots is due to their quantum-sized graphite structure<sup>12</sup>.

A mechanism known as the crosslink-enhanced emission effect (CEE) has been discovered using polymer dots (PDs). The potentially fluorescent centres of these PDs have their fluorescent properties amplified by the CEE effect. This is believed to be due to the decrease in rotation and vibration of the crosslinked PDs<sup>12</sup>.

A mechanism suggested by Sun *et al.* describes that the fluorescence of the C-dots is caused by surface energy traps that are present and become emissive after surface passivation<sup>26</sup>. It was theorised that the emissive energy traps experienced quantum confinement to the surface of the particles to allow the particle to have intense fluorescence properties after being surface passivated<sup>26</sup>.

### 1.1.3 Bioimaging with Carbogenic Nanoparticles

Research into C-dots is increasing, improving the imaging, diagnosis and treatment of various diseases as a result. Concerning this, materials at a nanometre scale must be synthesised and modified. With the use of these nanoparticles in drug delivery systems within the field of cancer medicine, results have shown an improvement in bioavailability, solubility, therapeutic

effectiveness, *in vivo* stability, intestinal absorption and the continual and targeted ability of many anticancer agents<sup>32</sup>.

C-dots have vast potential in the field of fluorescent bioimaging due to their great biocompatibility and low toxicity<sup>33</sup>. Research into how feasible C-dots were in mice as a fluorescence contrast led by Yang *et al.*<sup>34</sup>. This was done via subcutaneous injections of C-dots mixed into aqueous solution. Fluorescence images were then taken at different excitation wavelengths, with the green and red emissions contrasting sufficiently for imaging<sup>35</sup>. This same experiment has been repeated by Tao *et al.* giving similar results. The fluorescence imaging that followed was at seven excitation wavelengths between 455nm and 704nm (shown in **Fig. 1.2**). The best fluorescence contrast appeared at the 595nm excitation wavelength<sup>36</sup>.

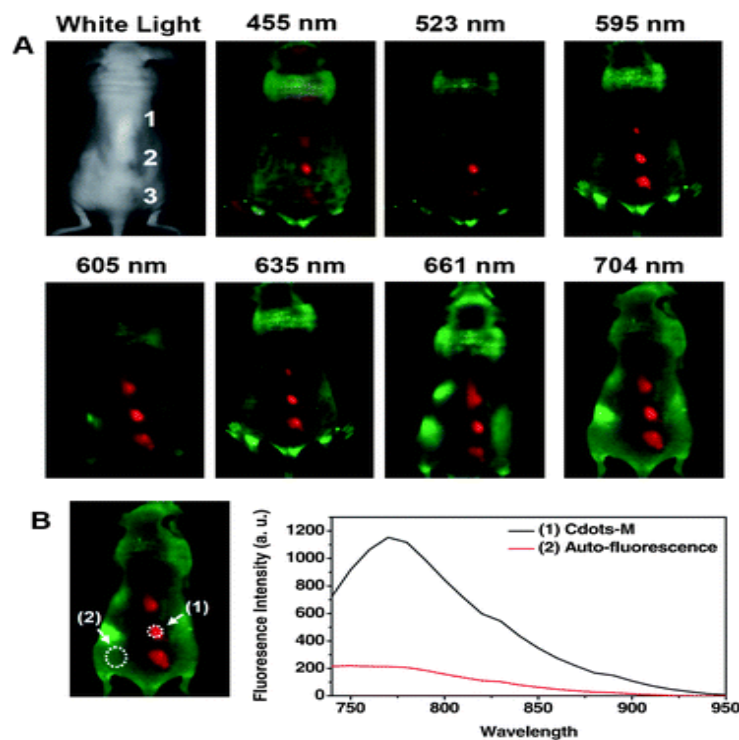


**Fig. 1.2.** *In vivo* fluorescence images upon the injection of C-dots subcutaneously into live mice, with various wavelength excitations. In addition, the fluorescence intensities at different excitation wavelengths are shown in a graph<sup>32</sup>.

The C-dots become highly fluorescent due to being surface-passivated by organic or biomolecules, and have now been found to be photo-chemically stable, physio-chemically stable and non-blinking<sup>37</sup>. The fluorescence of the carbon core within these C-dots can also be further improved via doping before the surface functionalization using an inorganic salt such as ZnS<sup>38</sup>. In addition, it has been shown by Wang *et al.* that the fluorescence properties of C-dots can also be enhanced via doping with nitrogen to result in structure effects<sup>39</sup>.

#### 1.1.4 Toxicity of Carbogenic Nanoparticles

Experiments on the cytotoxicity of carbogenic nanoparticles were investigated by Tao *et al.* This was done by exposing the human kidney embryonic 293T cell line to three varying types of C-dots to observe any *in vitro* toxicity effects. The varying C-dots were organised into different concentrations for each type of C-dot, they were then left to incubate for 24h in cells that were cultured in 96 well-plates. The cell viabilities were then tested after receiving the treatment of C-dots. It was shown that even at extremely high concentrations of C-dots (<0.5 mg/mL) the cell viability was not significantly affected. These results show that there are no obvious *in vitro* toxicity effects caused by C-dots (Fig. 1.3)<sup>40</sup>.

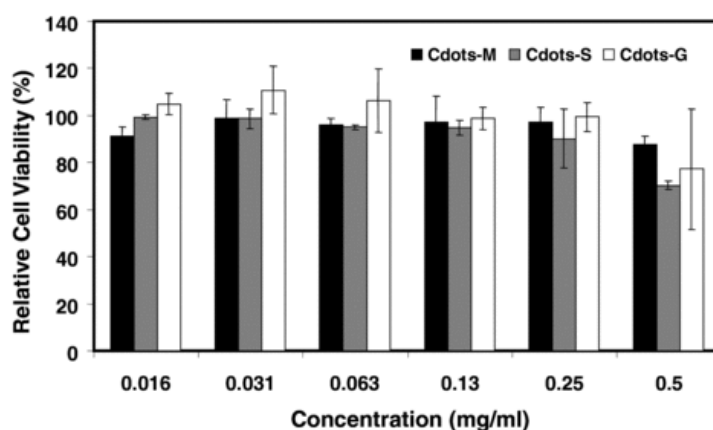


Fig. 1.3. Cell viabilities after exposure to various concentrations of three types of C-dots<sup>40</sup>.

The potential for the use of C-dots for *in vivo* and *in vitro* imaging applications is continually researched. Although, the toxic effects and toxicity levels of various C-dots have been studied, such as LD<sub>50</sub> (median lethal dose). It has been proposed that C-dots have a biocompatibility that

is comparable to dyes used in optical imaging agents that have been recently FDA approved. An example of these dyes is indocyanine green (LD<sub>50</sub> = 60 mg/kg bodyweight)<sup>34</sup>.

#### 1.1.5 Carbogenic Nanoparticles for Drug Delivery

There have been many examples recently showing that C-dots are very versatile and can be used in a vast array of areas with regards to drug delivery. The versatility of these particles can be seen in their ability to carry so many different types of drugs, with many scientists focusing on anticancer drugs as the ultimate objective. Examples of these anticancer drug carrying abilities can be seen below:

A study led by Zeng *et al.* showed fluorescent spherical C-dots with sizes ranging between 2 and 6 nm, that were green-emitting and had surfaces that were rich with carboxyl groups proved to be a working trackable delivery agent for cancer treatment that is localized in a mouse model. The normal cells and cancer cells had differing pH levels that could be used as the activating mechanism for the release of the drug Doxorubicin (DOX), which was conjugated via non-covalent bonding to the C-dots with the use of the amine moiety on the drug and the carboxyl groups on the C-dots. Even in biological systems that were complex, this stimuli-responsive non-covalent bonding proved to be adequately stable<sup>41</sup>.

Similarly, a study led by Feng *et al.* involving the use of fluorescent C-dots that had dispersion that was uniform with particle diameters ranging between 5 and 8 nm. These C-dots were used as drug nanocarriers that are imaging-guided, with an active targeting ligand known as RGD peptide, covered by monomethoxypolyethylene glycol (mPEG) via pH responsive benzoic-imine bond and cisplatin (IV) as the prodrug carried by the C-dots. Together, they form a pH/redox dual responsive type of C-dots that significantly enhance anticancer drug delivery and have targeting abilities that are triggered via tumour extracellular microenvironments<sup>42</sup>.

Furthermore, a study led by Karthik *et al.* describes the conjunction of a quinoline based photo-trigger with fluorescent C-dots to give a nano drug delivery system that is photo-responsive. The C-dots used had a particle diameter ranging between 5 and 7 nm, before being conjugated with an anticancer drug that could be photo-triggered known as 7-(3-bromopropoxy)-2-quinolylmethyl chlorambucil (Qucbl). Efficient anticancer drug release was observed through the exploitation of the photo-trigger ability of quinoline, with the use of both one-photon and two-photon excitation methods<sup>43</sup>.

## 1.2 Polymeric Prodrugs as a Model Drug Delivery System

Polymeric prodrugs can be described as inactive pharmaceutical agents that may transform enzymatically or chemically, forming an active parent drug within an organism after administration<sup>44</sup>. Some prodrugs remain inactive until they arrive at the desired site of action<sup>45</sup>. These drugs tend to be only one to two enzymatic/chemical steps away from the desired active parent drug, and as a result, they tend to be closely similar derivatives of the desired drug. In these materials, the drug release can be initiated by the cleavage of a chemical bond in drug delivery systems of a specific type<sup>44</sup>. Developments have been observed in the properties of pharmacologically active compounds via prodrug application. These properties include types such as physiochemical, pharmacokinetic and biopharmaceutical. It has been established at an estimate that approximately 10% of worldwide marketed drugs can be labelled as prodrugs, with a third of all approved small molecular drugs becoming known as prodrugs in 2008<sup>44</sup>.

The concept of polymeric prodrugs involves the use of designed novel agents, the aim of which is to accomplish selective activity at a specified target site, applying activation enzymatically that is specific to that site of action<sup>46</sup>. However, not all types of prodrugs have a carrier that is immediately obvious, thus revealing the requirement for molecular modification to generate a

new active compound. Various prodrugs specifically designed to overcome toxicity, formulation and delivery barriers to the application of drugs have reached the drug market<sup>47</sup>.

The desired goal of a prodrug is to conceal unwanted properties in the drug, these properties include: chemical instability, low solubility in water/lipid membranes, pre-systemic metabolism, toxicity, undesired taste, minimal target selectivity and local administration resulting in soreness or irritation<sup>48</sup>. There are three overlapping objectives to strive towards with regards to the research of prodrugs:

The first objective being pharmaceutical; improving the solubility of the drug, along with its chemical stability, organoleptic properties, to decrease problems that could be linked to the pharmaceutical technology of the active agent, and to diminish irritation and/or pain upon the administration of the drug<sup>49</sup>.

The second objective being pharmacokinetic; improving the amount of time the drug remains within a patient's body before degrading fully, along with the absorption of the drug, and to improve the tissue/organ-selective distribution of the active agent<sup>49</sup>.

The third objective being pharmacodynamic; reducing toxicity levels of the drug, advancing its therapeutic index as a result, and to form single chemical units containing multiple drugs<sup>49</sup>.

### 1.2.1 Structure of Polymeric Prodrugs

The synthesis of macromolecular prodrugs can be done by taking molecular drugs that are small and conjugating them covalently alongside polymeric carriers. It has been proven that these prodrugs result in a controlled and sustained release of a desired therapeutic agent *in vitro/in vivo*. Polyethylene glycol (PEG) is a good example of a prodrug that is macromolecular and has

been extensively used due to its low toxicity, high biocompatibility and low immunogenicity. However, PEG that is linear has a constant number of available hydroxyl groups through polymeric chain length changes. As a result, this means the PEG has limited application in purposes involving drug conjugation<sup>50</sup>.

In the Ringsdorf model of a polymeric prodrug there are five main components that make up the drug: the polymeric backbone, the solubilising group, the targeting group, the biodegradable spacer and the drug, as shown below (Fig. 1.4).

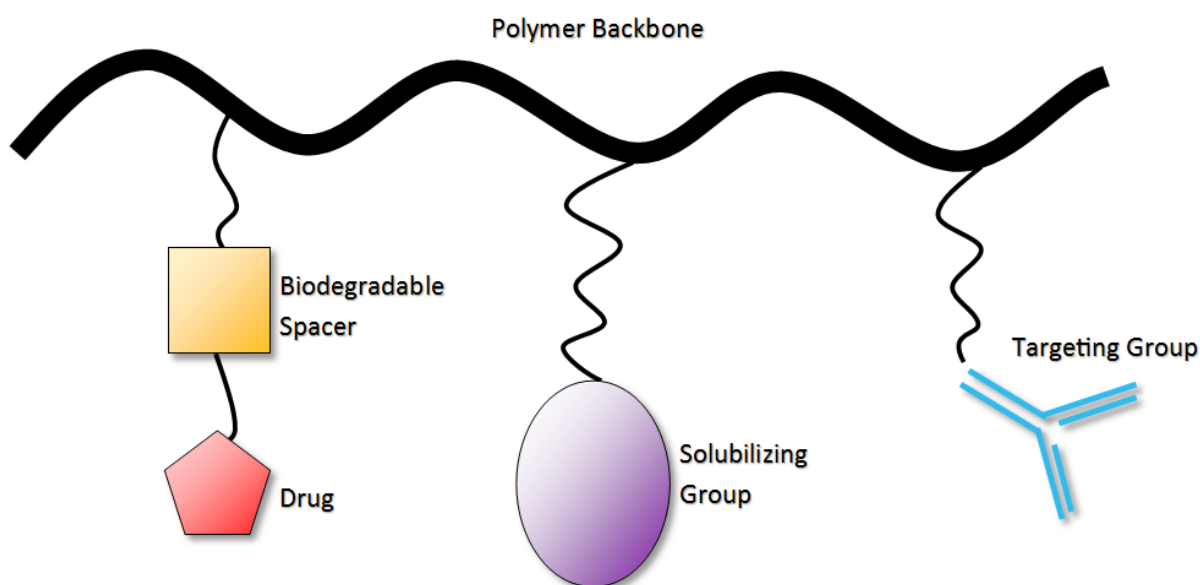


Fig. 1.4. Ringsdorf model of a polymeric prodrug<sup>52</sup>.

First, for the polymeric backbone to become a viable option in the prodrug due to its responsibility for drug delivery, certain criteria must be met. The functional groups in the polymer must be suitable in that they must be available for covalent coupling with drugs such as;  $-NH_2$ ,  $-SH$ ,  $-COOH$ , or  $-OH$ . The polymer must have a good water solubility, aka hydrophilic. The polymer should be readily available so that it can be manufactured at a sufficient capacity and must be properly administered to patients in need of the drug. The polymer must also be non-toxic, non-immunogenic, non-antigenic, biocompatible, and biodegradable and must have a molecular weight below the renal excretion limit. Finally, the final conjugates of the polymer must have an acceptable homogeneity, aka a low polydispersity<sup>51</sup>.

Second, the solubilising group is responsible for how soluble the drug is in water, and therefore must be a hydrophilic group<sup>52</sup>.

Third, the targeting group has the responsibility of making sure the polymeric prodrug reaches the desired site of pharmacological action. The targeting group has abilities that are dependent on a few different variables; the binding affinity for the ligand, the ligands internalization, non-antibody ligands or antibody fragments, and the choice of antibody<sup>53</sup>.

Fourth, the biodegradable spacer is responsible for monitoring the site of action and the dispersion rate of the active drug after it has been enzymatically/chemical activated via hydrolytic cleavage from the conjugate<sup>54</sup>.

Fifth, also the final component in the Ringsdorf model of a prodrug is the drug itself. The drug must remain covalently bonded to the polymer backbone until the macromolecule arrives at the desired site of action. Drugs that are chosen for this role must fit three important criteria: (1) the drug must be suitably stable and must not be released in conjugate form before arriving at the desired site, and only then should it be released. (2) There must be a functional group present in the drug that allows it to bind via a spacer or directly to the polymer backbone. (3) The amount of drug that can be administered is limited, therefore the drug must be very potent<sup>55</sup>.

### 1.2.2 Advantages of Polymeric Prodrugs

Polymeric prodrugs have various advantages. One example is that through circulation around the body, the drug will eventually reach a desired site of action, and only then will the drug be released at a controllable rate. The rate of release of the drug is controlled by having a specific type of linkage between the drug and the polymeric carrier, appropriate to the treatment. Controlling the release rate can be done in two ways, through pH or by the use of enzymes. With

the use of enzymes, the prodrug is taken up intracellularly, allowing the drugs to enter lysosomes that are present in healthy and tumorous tissues. The enzymes within the lysosomes then act on the polymeric prodrug, resulting in the active macromolecular drug being released<sup>56</sup>. The cytotoxic drug then destroys any tumour tissue with the help of the enzymes<sup>57</sup>. Control using pH involves the use of a pH sensitive linker such as *N-cis*-aconityl spacer, releasing the drug intracellular into tumour lysosomes or tissue when compared with healthy tissue<sup>58, 59</sup>.

Another example of an advantage of a polymeric prodrug is their permeability effect and enhanced retention. These prodrugs are passively absorbed by solid tumours via pinocytosis which improves the targeting ability of the drug<sup>60</sup>. The tumours have increased vascular permeability and have poor drainage from tissue cells, these properties are what allow for an increased action duration and targeting ability<sup>61</sup>.

The active targeting of polymeric prodrugs means that, via the endothelial cells, the angiogenic vessels of cells that are tumorous can be targeted. This is because the cell proteins appear to manifest at an increased level. Integrin receptors are present in these proteins along with receptors responsible for vascular endothelial growth factor (VEGF)<sup>62</sup>. There are potential targeting groups that are peptides that are able to bind to these receptors specifically and selectively<sup>63</sup>. Lectins can also be targeted using targeting groups in polymeric prodrugs because they are sugar specific receptors that are present in cells on the plasma membrane. Hepatocytes are an example of cell that these receptors are a characteristic of<sup>64</sup>.

The increased drug action duration in polymeric prodrugs is because of their slower renal elimination and because they are metabolically inactive. The length of action of these prodrugs is measured by plasma concentration, which is usually calculated as the area under curve (AUC). Through allowing the drug to link to a polymer, therefore obtaining a conjugate, the duration of

action can be extended. This slows down the endocytotic cell uptake, renal excretion and blood circulation of the drug<sup>65-67</sup>.

With polymeric prodrugs, the immunity of a patient can be protected because of a mechanism known as Fas-Fas Ligand (Fas L) interaction<sup>68</sup>. These ligands are present on cancerous and immune cells, and interacting with the Fas L can result in the apoptosis of a cell (death) via a torrent of signals<sup>69</sup>. Studies reveal that the stimulation of Fas L on cancerous cells can be encouraged with free anti-tumour treatment, but not with their macromolecular derivatives. These results show the potential of polymeric prodrugs with regards to the protection of a patients' immune system<sup>70</sup>.

### 1.3 Hydrogels as a Drug Delivery System

Hydrogels have a massive array of uses in a vast degree of fields such as drug delivery systems<sup>71</sup>, biomolecule or cell separation<sup>72</sup>, pharmaceuticals<sup>73</sup>, tissue engineering and regenerative medicines<sup>74</sup>, diagnostics<sup>75</sup>, biomedical applications<sup>76</sup>, biosensors<sup>77</sup>, wound dressing<sup>78</sup>, sealing<sup>79</sup> and regulating biological adhesions through becoming barrier materials<sup>80</sup>. Some gels can have a low water content, but typically hydrogels contain a large percentage of water (up to >90%) making them very biocompatible and these materials are physically or chemically crosslinked<sup>81</sup>. There are various ways to achieve this macromer crosslink; examples being through radiation exposure, temperature change or with the use of chemical crosslinkers<sup>82, 83</sup>. With the presence of a radical initiator, a chemical crosslink can be achieved when di-functional or multi-functional grouped crosslinking agent links to two or more monomer chains (shown in **Fig. 1.5**)<sup>84</sup>. These materials are excellent for drug loading due to their porous nature, and the rate of release of the drug is directly correlated with the diffusion rate of the hydrogel through the matrix. The density of the crosslink can also be controlled, allowing for the fine tuning of the rate of diffusion, resulting in continual drug release at a localized depot<sup>85</sup>.

On the other hand, hydrophilic drugs such as proteins have a higher probability to diffuse out of the gel due to the high water content of the hydrogels. This diffusion can happen in just hours, up to days<sup>86, 87</sup>. This problem can be solved using a cleavable linker, with the covalent binding of the hydrophilic drug to the hydrogel, thus increasing delivery time. As a result, the rate of release of the drug is directly correlated to the rate of hydrolysis of the cleavable linker<sup>86, 87</sup>.

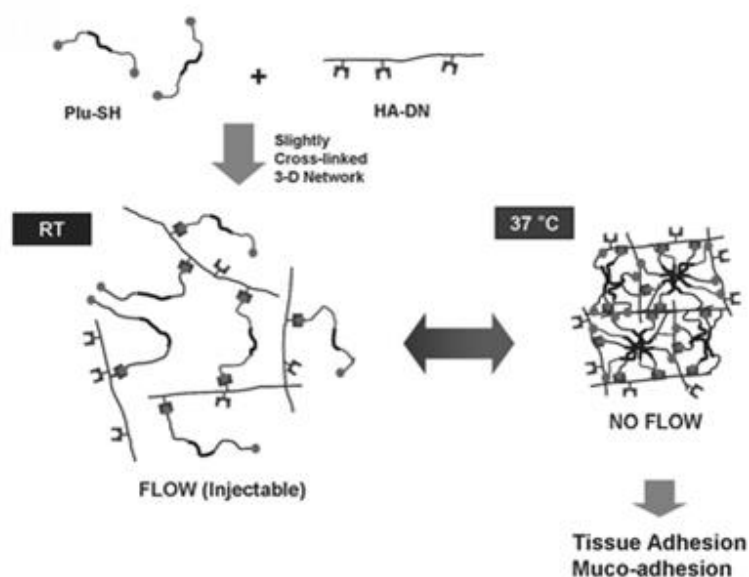


**Fig. 1.5.** HA/Pluronic<sup>®</sup> hydrogels slightly cross-linked 3-D network formation and their sol-gel transition characteristics<sup>88</sup>.

### 1.3.1 Types of Hydrogels and Categorisation

There are many types of hydrogels, which can be synthesised in a variety of ways and can be categorised through a number of ways. Hydrogels can be categorised based on what source they are from, being either synthetic or natural<sup>89</sup>.

They can also be categorised depending on their composition of polymers:

**(1)** Polymeric hydrogels that are Multipolymer Interpenetrating (IPN) are formed from two natural and/or synthetic polymer components that are independent of each other and are cross-

linked, contained in a form of network. These polymers can also have one being non-cross-linked and the other being cross-linked, making the hydrogel semi-IPN<sup>90</sup>.

**(2)** Hydrogels that are copolymeric consist of at one or more hydrophilic components with two or more monomer species that are different to each other, which have an alternating, block or random configuration arrangement along the polymer network chain<sup>91</sup>.

**(3)** Hydrogels that are homopolymeric, meaning one species of monomer making up the whole polymer network, which is the structural unit that is most basic. Depending on the technique of polymerization and the monomer nature, these types of polymers can have a cross-linked skeletal structure<sup>92</sup>.

Hydrogels can be categorised based on electrical charge absence or presence on the cross-linked chains. These hydrogels are organised into groups being zwitterionic where the structural repeating units have both cationic and anionic groups present. They can be an amphoteric electrolyte having both basic and acidic groups present. Finally, the hydrogels can be ionic or non-ionic in nature, meaning they have positive/negative charge or are neutral respectively<sup>93</sup>. They can also be classified according to their chemical composition and physical structure, being crystalline, amorphous (non-crystalline) or semi-crystalline which is a complex mixture of the two<sup>93</sup>.

### 1.3.2 Advantages of Hydrogels

Hydrogels have alternate methods of use when combined with other drug delivery methods such as liposomes or lipid microtubules<sup>94, 95</sup>. In microsphere systems, the drug is often released in a single burst, however, in hydrogel systems this does not occur and the drug particles may remain at the site of desired treatment. The release times of the hydrophilic molecules are increased by hydrophobic liposomes or microspheres<sup>96</sup>. Many hydrogels can transition into a gel *in situ* through an increase in temperature through body heat, this is because the polymers

have a lower critical solution temperature, thus forming a gel upon entry into the body. This phase transition process can be known as the sol-gel (lower) and gel-sol (upper) transitions. In addition, this phase transition is reversible in some gels<sup>97</sup>.

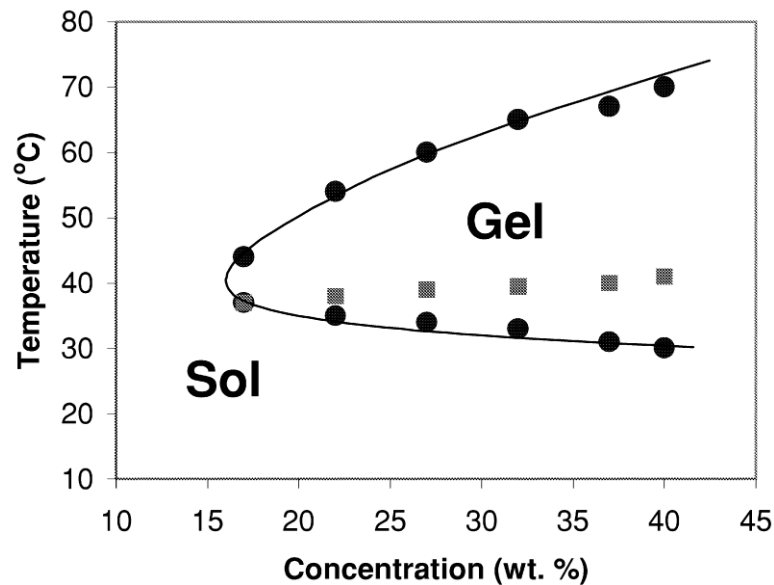


**Fig. 1.6.** Sol-gel phase diagram example of a triblock co-polymer in aqueous solution. The sol-gel transitions are shown as the circles, and the squares represent the temperatures at which the gel becomes turbid, acquired from references<sup>98</sup>.

In temperature sensitive gels, the sol-gel phase transition describes the temperatures at which a specific type of polymer gel changes from a solution to a gel. More specifically, triblock co-polymer gels transition from a solution to a gel at body temperatures (around 37°C) and can transition back to a solution again at higher temperatures, as shown above (**Fig. 1.6**). The lower sol-gel transition mechanism is known to be caused by the increasing amount of micelles that form as the temperature increases, which then aggregate together, giving rise to a more closely packed system (gel). On the other hand, the upper gel-sol transition occurs when the temperature continues to increase further, causing the hydrogen bonds between the PEO chains and the water molecules that are present to get weaker, thus resulting in de-swollen micelles and the removal of the close packing constrains. It was observed that as the

hydrophobicity of the triblock co-polymers increased, the critical gel concentration and sol-gel transition temperatures decreased<sup>99</sup>. Alternatively, polymers such as alginate or chitosan form gels through either the addition of salts or pH changes due to their ionic interactions<sup>100</sup>.

On the other hand, hydrogels can be synthesised via light induced formation. This is done through monomers being exposed to a photo-initiator, which are compounds that are sensitive to light and generate free radicals when exposed to light in the UV/vis range, thus commencing polymerization via active sites on macromer chains as a result<sup>101, 102</sup>. With regards to photopolymerization, the spatial and temporal dimensions can be tuned in the process of polymerization, giving it advantages over other types of polymerization<sup>103</sup>. Prior to polymerization, the desired shape of construct can be achieved using a mould or defect of choice due to the liquid form of the polymer. A specific gelling depth can also be achieved via changes in light intensity and exposure time. Appropriate bioactive cells or factors can also be mixed with the photo-curable hydrogels upon injection using a syringe, much like temperature or chemical crosslinking<sup>103-107</sup>. In addition, the delivery system will be completely eliminated from the body after a period of time if biodegradable or bioresorbable materials are used for the synthesis of the hydrogels<sup>108</sup>. Hydrogels have further advantages within the field of tissue engineering specifically because they decrease the number of surgical procedures required to treat an illness, improving the morale of patients<sup>109</sup>.

### 1.3.4 Fluorescent Dyes in Hydrogels

Through the addition of fluorescent microbeads, hydrogels have the capacity to become fluorescent. A recent study revealed that these types of hydrogels have huge potential for *in vivo* glucose monitoring, uninterrupted, with wireless transdermal transmission and a long lasting activity<sup>110</sup>. These fluorescent materials are not yet understood deeply enough as they still have a lacking intensity in transdermal transmission and maternal toxicity. A study led by Hideaki *et al.* showed a fluorescent monomer was synthesised that had polymerization sites, glucose-recognition sites and a fluorogenic site<sup>110</sup>. The spacers were designed to be long and hydrophilic in an attempt to allow more glucose molecules to bind to the monomer. Therefore these fluorescent monomers result in a high-intensive responsiveness to glucose. Fluorescent polyacrylamide hydrogel beads that were injectable-size were synthesised that had high throughput and high uniformity. It was established that these fluorescent microbeads had a sufficient fluorescent emission intensity to transdermally monitor concentrations of glucose *in vivo*<sup>110</sup>.

Alternatively, a study led by Wang *et al.* showed the building blocks of a polymer being joined together with a DNA template, forming a DNA-conjugated polymer composite hydrogel. The delocalised electron structure of the conjugated polymer caused the hydrogel to exhibit fluorescence. This fluorescence was shown to be quenched by the addition of a drug, and this fluorescence returned once the drug had been dispersed. These characteristics show very useful applications for scientists, as they can view and keep track of the hydrogel fluorescence during *in vitro* experiments, revealing information on the amount of drug that a hydrogel will be likely to distribute after administration on humans<sup>111</sup>.

## 1.4 Pluronic® Surfactants for Preparing Hydrogels

The term 'Pluronic®' is used to describe triblock copolymers that are water soluble, with the structure PEO-PPO-PEO. The PEO is an abbreviation of poly(ethylene oxide) and PPO of poly(propylene oxide). It is their potential intrinsic biological activity and already attractive fundamental properties that are responsible for the extensive use of these amphiphilic block copolymers in the field of nanomedicine<sup>112</sup>. Modifying the molar mass ratio between the PPO and PPE can alter the interactions that these Pluronic® copolymers have with cell membranes/cells and can change the *in vivo* properties. This allows for the fine tuning of their chemical and physical properties, creating growing prospects for the design of novel biomaterials and innovative nanomedicines<sup>112</sup>.

These materials are formed by micelles above the critical micelle concentration (CMC). These compounds are non-ionic surfactants that are highly active on the surface<sup>113, 114</sup>. The highly temperature-dependant nature of the propylene oxide and ethylene oxide blocks will result in the triblock copolymer being formed, when the CMC is dropped drastically through an increase in temperature<sup>115</sup>. The parameter used with regards to micelles is known as the critical micellar temperature (CMT), and the process of micellisation is reversible<sup>115</sup>, as shown below (**Fig. 1.7**). Pluronics® consist of two outer shells of PEO blocks that are hydrophilic, surrounding a hydrophobic core in the form of PPO that is weakly hydrated<sup>116</sup>, resulting in a copolymer that is amphiphilic<sup>117</sup>. In the micellisation process, the triblock copolymers rise to the surface of the water, and only once this layer has formed on top of the water will micelles begin to be formed<sup>117</sup>.

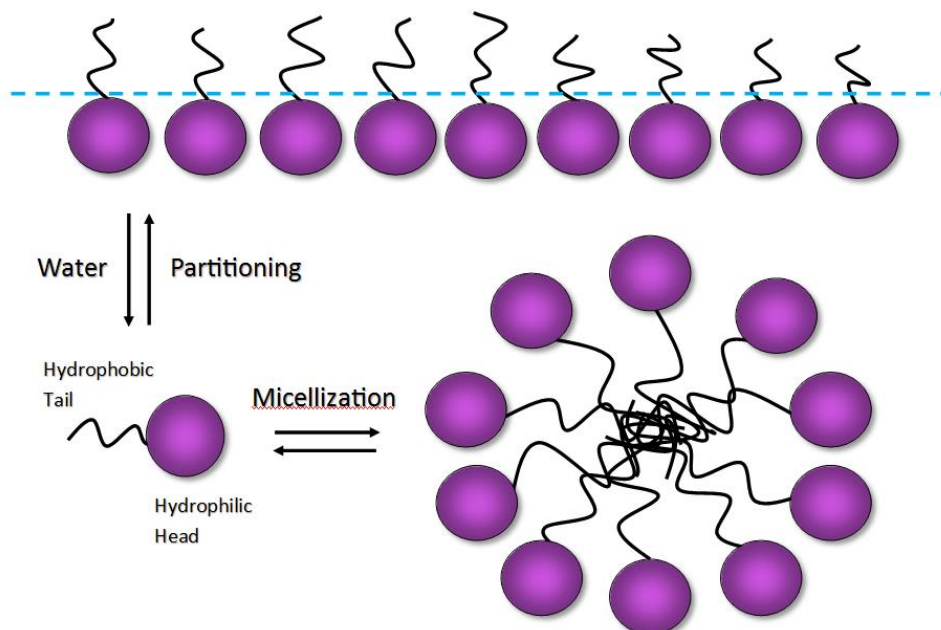


**Fig. 1.7.** Formation of micelles as an overall mechanism for polymers. In triblock copolymers there will be two hydrophobic tails representing the PEO in PEO-PPO-PEO<sup>118</sup>.

There are a few factors that can change the type of block copolymer that is formed, such as block size, temperature, solvent composition and molecular weight<sup>118</sup>. Pluronics® that have a higher molecular weight are usually formless solids, whilst those with a lower molecular weight tend to be creams or oils<sup>118</sup>. The presence of impurities and high hydrophobic constituents can be seen when Pluronics® behave abnormally, which can be attributed to the solvents that are chosen or exposure to unsuitable temperatures<sup>116, 119</sup>.

#### 1.4.1 Self-Assembly in Water

The property that defines the term Pluronic® is the capability of the 'unimers', alternatively named as individual copolymer molecules, to undergo micellisation in aqueous solution. When the concentrations of the block copolymer are lower than the CMC, the 'unimers' form a molecular dispersion. Alternatively, micellisation will occur if the concentration of the block copolymer is higher than the CMC. It is the interactions of the PO blocks that are hydrophobic in nature that is the reason that micellisation happens. These hydrophobic PO blocks assemble themselves into the inner core of micelles, and the hydrophilic corona of the EO blocks is what

surrounds them. This structure setup is usually depicted as a sphere for most block copolymers, when >30% of EO block content is present. This especially applies at body temperature with relatively dilute solutions. Depending on the type of Pluronic® used, the spherical micelles that form usually have a different average hydrodynamic diameter, varying from 20 up to 80 nm<sup>118</sup>. In addition, the number of ‘unimers’ that form into a single micelle can change from a few to over a hundred, this is known as the ‘aggregation number’<sup>120</sup>.

#### 1.4.2 Drug Solubilisation and Delivery

Polypeptides and low molecular mass drugs are being investigated when solubilized into the Pluronic® micelles<sup>121</sup>. Solubilisation is the term used to describe the process of transferring water-insoluble compounds into the hydrophobic core of the micellar solution<sup>122-125</sup>. These polymeric micelles are effective carriers of compounds that typically would have undesired pharmacokinetics, low stability and poor solubility in a physiological environment. This is because of their essential core-shell architecture. The pharmaceutical behaviour of the block copolymer is improved greatly by the hydrophilic shell, allowing the micelles to maintain in a dispersed state, along with reducing the amount of unwanted interactions of the drugs with proteins and cells via steric-stabilization effects. In addition, the water-incompatible hydrophobic core formed by the PO chains create a sort of ‘cargo hold’ for specific therapeutic reagents that would otherwise not be feasible in these types of treatment (**Fig. 1.8**).

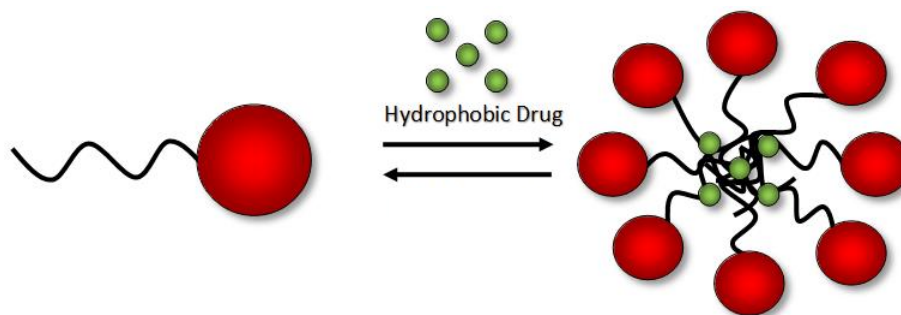


**Fig. 1.8.** Drug loading of a typical micelle 'unimer' using a hydrophobic drug. This is done via self-assembly<sup>126</sup>.

A polymeric micelle that is perfect for the job must show appropriate biological stability and compatibility, a great loading capacity and monitored drug release. However, the polymeric micelles have physicochemical characteristics that are completely dependent on the properties and lengths of the hydrophilic and hydrophobic blocks<sup>126</sup>. This results in an improved metabolic stability, solubility and circulation release time period of the drug<sup>127</sup>. Upon administration of the drug, the micelle concentration will rapidly decrease down to below the CMC, resulting in the concentration of the therapeutic agent decreasing also. However, it should be known that stability is compromised<sup>127</sup>.

## 1.5 JEFFAMINES® for Functionalisation of C-dots

Alternatively named as 'polyetheramines', these molecules consist of a polyether backbone with primary amino groups attached to each end. Propylene oxide (PO) and/or ethylene oxide (EO) are normally the constituents of the polyether backbone, giving the name 'polyetheramines'<sup>128</sup>.

Up until recently, the JEFFAMINE® family contained core structures that were primarily monoamines, diamines and triamines. However, this unique range of product now has improved utility, with polytetramethylene glycol (PTMEG) based JEFFAMINES® emerging<sup>128</sup>. The diamine JEFFAMINES® have EDR, ED, and D series products. These molecules are defined and named with their molecular weight, with the D Series JEFFAMINES® named as D230 or D400 for example, with the D signifying a diamine. The EDR signifies a PEG based diamine that is highly reactive, and the ED represents a diamine with a predominantly PEG backbone. However, the D Series JEFFAMINES® are the only series that will be studied in this project, and are amine terminated PPGs with the following representative structure (**Fig. 1.9**)<sup>128</sup>, with the x indicating the number of repeats along the polymer backbone:

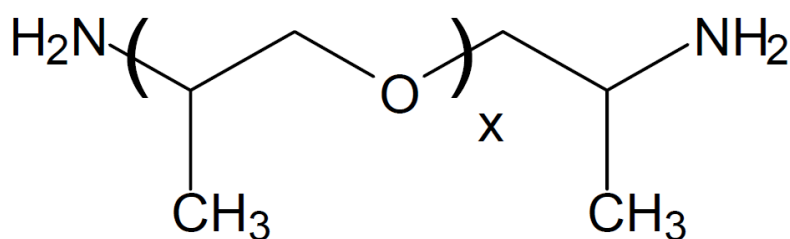


**Fig. 1.9.** D Series JEFFAMINE® representative structure<sup>128</sup>.

These polyetheramines usually engage in typical amine reactions, regularly showing low viscosity and colour, increased toughness and increased flexibility. The variables in these JEFFAMINES® include different repeating unit types, distribution, amine functionality and

varying molecular weight, resulting in the designing of new mixtures or compounds to be very flexible<sup>128</sup>.

### 1.6 Paracetamol for Drug Release Profiles

Paracetamol (PCL) is known as a mild analgesic and anti-pyretic drug<sup>129</sup>. It has the chemical name para-acetylamino phenol, shown below (**Fig. 1.10**). It has insignificant anti-inflammatory properties, but is an effective and regularly used drug to treat fever and pain<sup>130</sup>. This drug is typically administered orally or rectally, and is soluble in water. However, it has a low solubility in water in comparison to other polar solvents such as alcohols<sup>131</sup>. The side effects of an overdose of PCL include a loss of appetite, diarrhoea, nausea, increased sweating, stomach cramps/pain, and swelling/pain/tenderness in the upper abdomen area<sup>132</sup>.

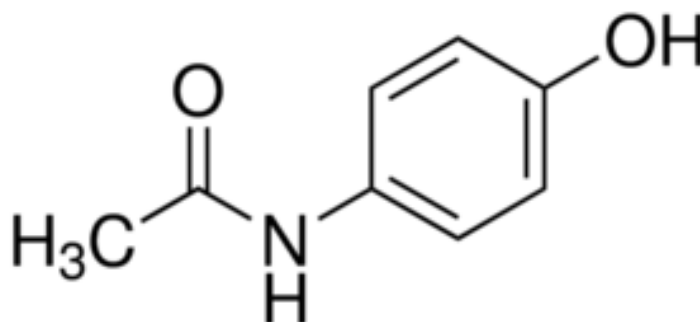


**Fig. 1.10.** The chemical structure of Paracetamol (para-acetylamino phenol)<sup>134</sup>.

Paracetamol is absorbed very effectively in the gastrointestinal tract. However, bioavailability via oral administration is dependent on the dose. The highest concentration of the drug in blood plasma is reached within less than two hours. Paracetamol also has a half-life of two and a half hours, resulting in the need for regular doses to maintain the therapeutic effect for longer periods of time<sup>133</sup>.

## 1.7 Ibuprofen for Drug Release Profiles

Ibuprofen (IBU) is classified as a non-steroidal anti-inflammatory drug (NSAID). Although its commercial name is widely used, this drug has the chemical name of 4-isobutyl- $\alpha$ -methylphenylacetic acid<sup>135</sup>, shown below (**Fig. 1.11**). IBU is primarily recognised for its anti-inflammatory, anti-pyretic and analgesic properties<sup>136</sup>. It is much more soluble in most organic solvents in comparison to water<sup>137</sup>. Primarily ingested orally, IBU can reach peak plasma concentration in two hours with the use of conventional tablets. With a half-life of 2 hours, regular doses of the drug must be administered to maintain therapeutic effect, similarly to paracetamol<sup>136</sup>.

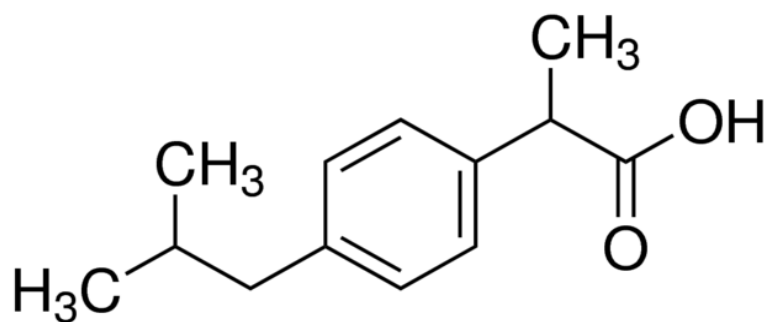


**Fig. 1.11.** The chemical structure of Ibuprofen (4-isobutyl- $\alpha$ -methylphenylacetic acid)<sup>139</sup>.

With both drugs having issues maintaining therapeutic effect for longer periods of time, the incorporation of a polymeric prodrug can be done by covalently attaching it to the drug via chemical or physical linkage, allowing for the release of the drug to be monitored<sup>138</sup>.

The drugs ibuprofen and paracetamol were chosen as examples of model drugs, to study the potential interactions that the C-dots have with the release profiles of these drugs.

## 1.8 Research Project Objectives

The objective of this study will be to synthesise the EA-CA carbogenic nanoparticles and to functionalise them with various types of JEFFAMINES<sup>®</sup>, to use them in conjunction with Pluronic<sup>®</sup> P-123 32.5 wt% hydrogels as a drug carrier. These types of C-dots will be used due to their fluorescence properties, biocompatibility and as a potential medium to control the release rate of model drugs. In addition, the fluorescence characteristics of these varying types of C-dots will be tested and compared. The functionalisation of C-dots with JEFFAMINES<sup>®</sup> will represent the polymeric backbone in a drug delivery system that will be similar to that of a polymeric prodrug.

Finally, therapeutic drugs ibuprofen and paracetamol will represent model drugs to be incorporated into a polymeric prodrug system. They will be dispersed into Pluronic<sup>®</sup> gels with different types of C-dots, to produce various drug release profiles also to be compared. This project will be an attempt to achieve controlled and sustained drug delivery whilst simultaneously allowing for real-time *in vivo* imaging to track the drug the location desired for therapeutic effect.

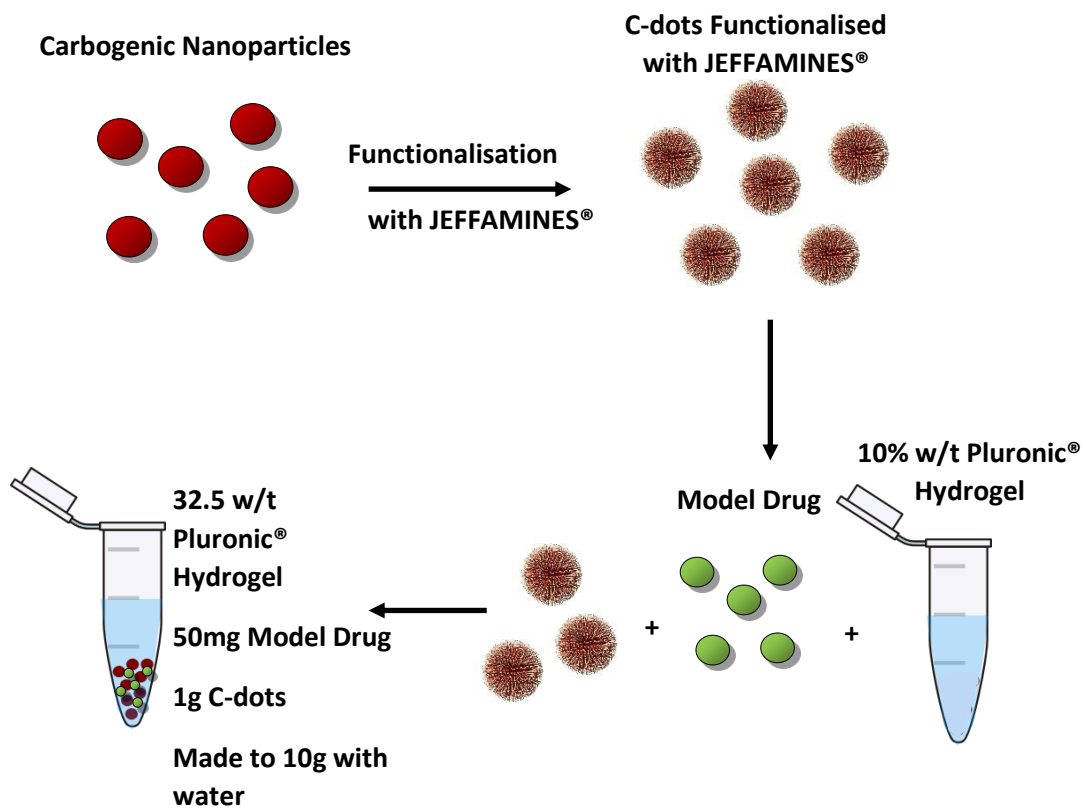


**Fig. 1.12.** Schematic drawing illustrating the experimental process in this research project.

## 2. Materials and Methodology

### 2.1 Materials

Sodium Phosphate Dibasic ( $\text{Na}_2\text{HPO}_4$ ) and Ibuprofen (4-isobutyl- $\alpha$ -methylphenylacetic acid) both bought from **Alfa Aesar, UK**.

JEFFAMINES<sup>®</sup> D-230 and D-400 were provided by **Alfa Chemicals, UK**.

Nitric acid 70% ( $\text{HNO}_3$ ) and Citric Acid Monohydrate ( $\text{C}_6\text{H}_8\text{O}_7 \cdot \text{H}_2\text{O}$ ) were both bought from **Fisher Chemical, USA**.

Ethanolamide  $\geq 98\%$  ( $\text{C}_2\text{H}_7\text{NO}$ ), and PEG-PPG-PEG, Pluronic<sup>®</sup> P-123 (average  $M_n \approx 5800$  g/mol) were both bought from **Sigma Aldrich, USA**.

Distilled, purified and deionised water taken from Elgastat Option 3 Water Purifier which was bought from **ELGA LabWater**.

SnakeSkin<sup>®</sup> Dialysis Tubing, Internal diameter of 35 mm and a molecular weight cut-off of 3.5 kDa was bought from **Thermo Scientific, USA**.

### 2.2 Methodology

#### 2.2.1 Carbogenic Nanoparticles Synthesis (aC-dots)

The protocol followed to synthesis the carbogenic nanoparticles in this research project was previously discovered by Marta Krysmann, Antonios Kellarakis *et al.*<sup>7-8</sup> prior to the beginning of this research project. The same protocol was repeated in this project, and is as follows:

With the use of a magnetic stirrer, 15ml of ethanolamine (EA) and 16.80g of citric acid monohydrate (CA) were mixed together in a round bottomed flask. This mixture of EA and CA was then initially heated using a hotplate at 180°C with a reflux condenser and left to reflux for 30 minutes. After this time had passed, the mixture was heated for a further 60 minutes at 230°C, and the reflux condenser was removed. The mixture was then transferred to a porcelain crucible whilst still hot and in liquid phase, to avoid solidification of the solution in the round

bottomed flask. This negates the need for water to be added to the mixture. This mixture was then calcined in the oven for 1 hour at 300°C.

After the mixture was removed from the oven and left to cool to room temperature, what remained was a carbonaceous material that needed to be ground down with the use of a mortar and pestle. The now crushed solid particles were ran through a micro sieve with a mesh size of 500µm to leave much smaller particles. These acquired carbogenic nanoparticles (CNPs) were dispersed in water and refluxed with nitric acid at 100°C for 16 hours. The solution formed was then filtered with standard filter paper to remove big agglomerates, and then placed in a centrifuge to facilitate the filtration step by further separating the CNPs from the big agglomerates.

In the filtration step, the solution of CNPs is filtered using a nitrate membrane filter leaving particles that are 0.45µm in size. This filtered solution was then placed in dialysis tubing, which was placed in 2.5L of distilled water and left to pass through the tubing until the CNPs were purified by the removing impurities and by-products. The distilled water was replaced once per day and the purification process would take from a few days up to a couple of weeks to complete. The now pure solution was then stored in plastic bottles and frozen. After being left in the freezer for 24 hours, the bottles were placed in a freeze dryer, which took around 5 days to become completely dry and ready to be used in this research project.

### 2.2.2 Functionalisation with JEFFAMINES®

The method used to functionalise the C-dots with JEFFAMINES® involved the addition of 7g of JD-230 and JD-400 into two separate round bottomed flasks. Each JEFFAMINE® was mixed with 5mL water with 0.2g of C-dots dissolved within it. Each mixture was heated to a temperature that was below the flash point of that corresponding JEFFAMINE® (128°C for D-230 and 163°C

for D-400)<sup>107</sup> without a reflux condenser for 3 hours using a C-MAG HS7 hotplate. This was done to evaporate all of the water from the mixtures.

Upon completion of the heating process, the mixtures were left to cool down to room temperature and then dispersed in water again to be placed in a Carbolite<sup>®</sup> furnace to be heated at 80°C for a few days until all water had evaporated again.

The substance that remained was left to dialyse against deionised water using SnakeSkin<sup>®</sup> dialysis tubing. The water in the dialysis was replaced with fresh water multiple times per day, until no more impurities came out of the dialysis tubing. The purified products were then transferred into sample bottles to be freeze-dried until they were completely dry.

### 2.2.3 Encapsulation of C-dots in Hydrogels

The Pluronic<sup>®</sup> gels that were to have C-dots functionalised with JEFFAMINES<sup>®</sup> present had 15 mg of the solid carbogenic nanoparticles added to 1g of Pluronic<sup>®</sup> gel and 9g water. The aC-dots were in solution at a concentration of 15.9 mg/ml, so 0.973 mL was used for each gel sample with aC-dots to make 15 mg/ml the standard concentration. The weight of the aC-dots solution was made up to 9g with water, and then 1g of P-123 was added to reach 10% w/t. The concentrations of the C-dots that were used in the pluronic gels were maintained at 15 mg/ml throughout the project.

### 2.2.4 Gel Phase Behaviours

The 32.5 wt% Pluronic<sup>®</sup> P-123 hydrogel were heated from 5°C to 80°C to distinguish the sol-gel and gel-sol phase transition temperatures, and to define the point at which the gels become turbid. The heating was done using a Grant Optima TC 120 circulation water bath.

### 2.2.5 Fluorescence Behaviours

The Pluronic® P-123 32.5% w/t hydrogels with various types of C-dots were exposed to long wave UV light at a wavelength of 365 nm using a Model CM10A Fluorescence Analysis Cabinet (Spectroline) to test and photograph their fluorescent behaviour. In addition, using a Fluoromax-4 Spectrofluorometer (Horiba Jobin Yvon), the aC-dots were ran through solid-like state fluorescence at 0.103 mg/ml in 32.5% w/t Pluronic® P-123 32.5% w/t. The samples were tested for their fluorescence properties at different excitation wavelengths (300, 340, 380, 420, 460, and 500 nm).

The different types of C-dots were also analysed with liquid state fluorescence at various excitation wavelengths (320, 350, 380, 410, 440, 470 and 500 nm). Each sample of C-dots was maintained at a concentration of 0.05 mg/ml. In addition, fluorescence microscopy images were obtained at three excitation wavelengths (350, 395 and 590 nm) using a Zeiss Axio Scope A1 Microscope with band-pass filters. The images that taken were compared with those of water.

### 2.2.6 Pluronic® Hydrogel Preparation and Drug Loading

As a standard, the hydrogels were made to 32.5% w/t using Pluronic® P-123 with a total mass of 10g. This gel was tested with different types of C-dots, observing the interactions of the C-dots with primarily Ibuprofen and some testing with paracetamol.

Ibuprofen will not disperse in the 32.5% w/t hydrogel so a 10% w/t gel must be made first to allow the drug to fully disperse and then the gel will be made up to 32.5% w/t. As it is very difficult to measure out 5mg of a drug without error, the mass of the total solution with the drug is multiplied by 10 up to a total of 10g with 50mg of drug. The 10% w/t was synthesised by adding P-123 to water at a ratio of 1:9 (1g P-123 to 9g water). Once the polymer had dissolved in the water, 50mg IBU was added and stirred using a magnetic stirrer until the drug had

completely dispersed. The hydrogel was made up to 32.5% w/t by adding a further 2.25g of P-123 and then also stirred until the polymer had completely dispersed, leaving a gel at room temperature, but a solution when cold.

To synthesise the hydrogel with ibuprofen or paracetamol, the same protocol is followed but the drug is added when the gel is at 10% w/t to allow the drug to disperse properly. Furthermore, the same protocol is also followed when using the various types of C-dots (aC-dots, JD-230 C-dots and JD-400 C-dots), all of which are shown below (**Table. 2.1**).

**Table 2.1.** *The masses used to synthesise Pluronic® hydrogels with varying C-dots and drugs.*

<b>Pluronic® Gels</b>	<b>P-123 added to make 10% w/t (g)</b>	<b>Drug Loaded (g)</b>	<b>C-dots Added (g)</b>	<b>P-123 added to make 32.5% w/t (g)</b>
<b>P-123 32.5% w/t</b>	1g	-	-	2.25g
<b>P-123 32.5% w/t + IBU</b>	1g	50mg IBU	-	2.25g
<b>P-123 32.5% w/t + aC-dots</b>	1g	-	1g aC-dots 2% w/t	2.25g
<b>P-123 32.5% w/t + JD-230 C-dots</b>	1g	-	1g JD-230 C-dots 2% w/t	2.25g
<b>P-123 32.5% w/t + JD400 C-dots</b>	1g	-	1g JD-400 C-dots 2% w/t	2.25g
<b>P-123 32.5% w/t + aC-dots + IBU</b>	1g	50mg IBU	1g aC-dots 2% w/t	2.25g
<b>P-123 32.5% w/t + aC-dots + P</b>	1g	50mg PCL	1g aC-dots 2% w/t	2.25g
<b>P-123 32.5% w/t + JD230 C-dots + IBU</b>	1g	50mg IBU	1g JD-230 C-dots 2% w/t	2.25g
<b>P-123 32.5% w/t + JD400 C-dots + IBU</b>	1g	50mg IBU	1g JD-400 C-dots 2% w/t	2.25g

### 2.2.7 *In Vitro* Drug Release Studies

These drug release studies were done at room temperature ( $20 \pm 1^\circ\text{C}$ ), with Pluronic<sup>®</sup> hydrogels at 32.5 w/t using P-123. The studies were also done with and without the presence of various types of C-dots. The hydrogels when synthesised were moved separately into their own SnakeSkin<sup>®</sup> Dialysis Tubing membrane. Each dialysis tubing membrane was placed into individual beakers with 200mL of buffer solution at 7.4 pH (citric acid monohydrate and sodium phosphate dibasic) and at room temperature.

The molecular weight of the P-123 when compared to the dispersed drugs is drastically larger, therefore the drugs were able to pass through the membrane into the buffer solution whilst the polymer could not. Samples of 1ml were taken from the solution surrounding the tubing, then placed in a glass sample vial, and the new volume was noted down to compensate for potential changes in concentration. These samples were taken at various time intervals at an attempt to plot a graph of drug release (0.25h, 0.5h, 0.75h, 1h, 2h, 3h, 4h, 24h, 48h, 72h, 96h 120h, and then every 3 days until the drug was 100% released).

All samples taken were ran through a UV-3600 Spectrophotometer (Shimadzu) over a range of 230-600 nm, and the concentration IBU that was released through the membrane was calculated. This calculation was done by plotting the levels of absorbance at the UV absorbance peak of IBU ( $\lambda_{\text{max}} = 263 \text{ nm}$ ) against an IBU calibration curve.

The calibration curve was devised by taking various concentrations of IBU ranging between 0.01 and 0.9 mg/ml, then analysing their absorbance levels through the UV-Vis 3600 and plotting the spectra at  $\lambda_{\text{max}} = 263 \text{ nm}$  (as shown in **Fig 2.1**).

The samples were analysed in quartz cuvettes with 1.0 cm path length. These spectrums were plotted against a sample of the 7.4 pH buffer that was used in the dialysis as a blank. All samples were analysed at room temperature.

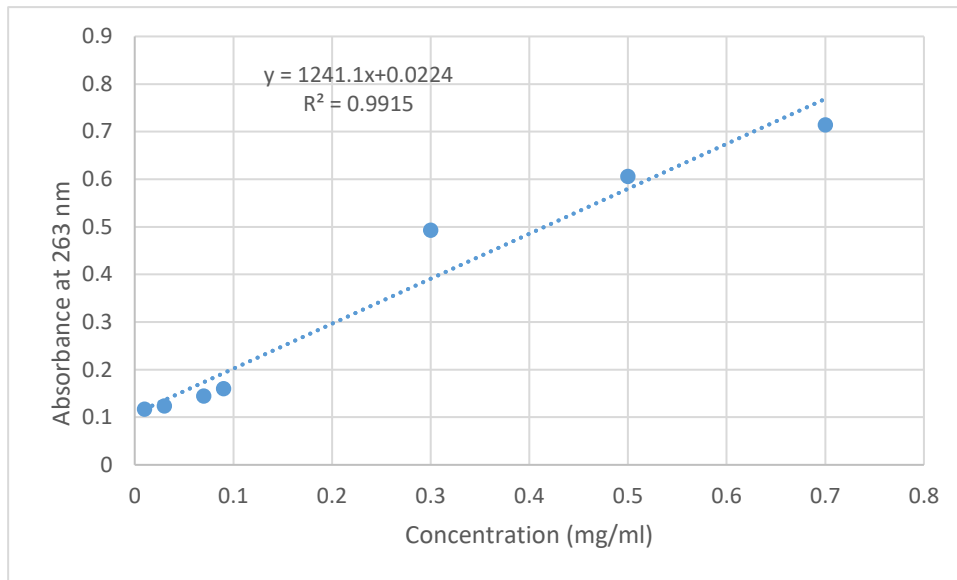


**Fig 2.1.** *Ibuprofen calibration curve using various concentrations of IBU (0.01, 0.03, 0.05, 0.07, 0.09, 0.1, 0.3, 0.5, 0.7, 0.9) in a phosphate buffer solution at pH 7.4. Absorbances taken at 263 nm as determined by UV-vis spectra in conjunction with literature.*

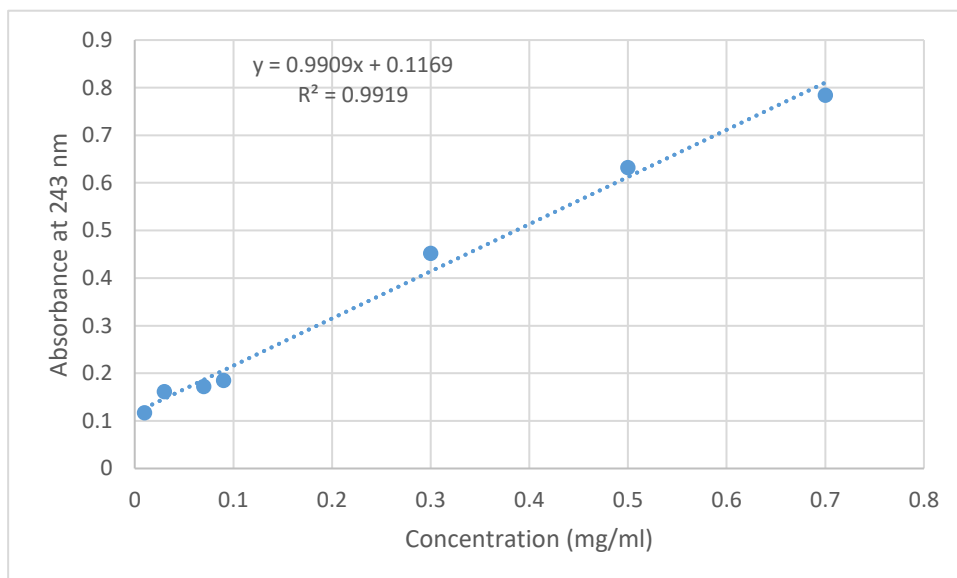


**Fig 2.2.** *Paracetamol calibration curve using various concentrations of PCL (0.01, 0.03, 0.05, 0.07, 0.09, 0.1, 0.3, 0.5, 0.7, 0.9) in a phosphate buffer solution. Absorbance taken at 243 nm as determined from UV-vis spectra in conjunction with literature.*

### 3. Results and Discussion

#### 3.1 Characterization of Carbogenic Nanoparticles

The protocol using citric acid and ethanolamine was followed to synthesise the C-dots that were used in this research project. This type of C-dot was abbreviated as aC-dots for purposes of efficiency. They have been previously characterised by Antonios Kelarakis, Marta Krysmann *et al*, confirming the legitimacy of their synthesis in this project.

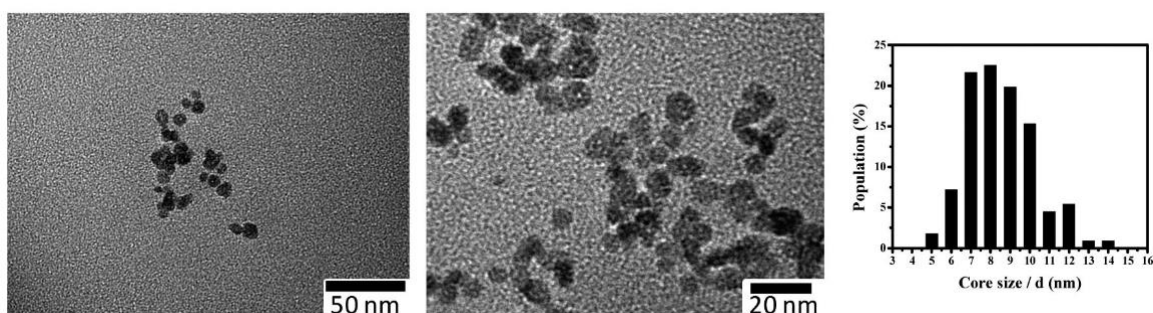


**Fig. 3.1** Tunnelling Electron Microscope images of the C-dots that were synthesised using the protocol in this project, and size histograms. Acquired from Reference<sup>3</sup>.

The synthesis of these C-dots was done with citric acid monohydrate and ethanolamine under pyrolysis at increasing temperatures (see methodology, p. 37), and resulted in the formation of carbogenic nanoparticles that have an average diameter of 8 nm (shown above in **Fig. 3.1**). These results concur with previous reports of C-dot synthesis using different pyrolysis methods<sup>140-144</sup> and the size of these C-dots stay consistent even when exposed to major chemical changes. It is shown via TGA-MS experiments that in this system, a massive amount of carbon dioxide escapes during the 300°C stage of pyrolysis, which is accountable for the great reduction in size of the C-dots. Looking at the elemental analysis, the C-dots after being exposed to 300°C have a reduced amount of hydrogen and an increased amount of carbon when compared to the C-dots at 230°C, with a chemical composition of 50.5% C, 3.7% H and 13.1% N<sup>3</sup>.

The C-dots appear to have a number of functional groups on their surface, due their capability to be well dispersed in water. This can be confirmed by looking at the FTIR spectra (shown below in **Fig 3.2**), showing that even after treatment at such a high temperature, there are clearly stable imide and amine groups remaining. However, the amount of these groups is significantly reduced when compared to the C-dots during pyrolysis prior to the 300°C stage of the process.

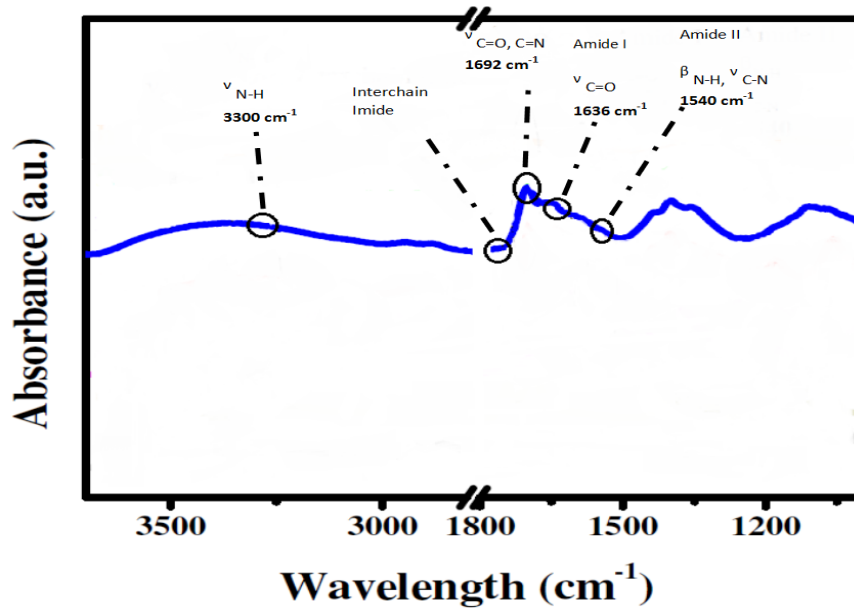


**Fig. 3.2.** FTIR spectra to show the presence of imide and amide functional groups on the surface of the C-dots. Acquired from reference<sup>3</sup>.

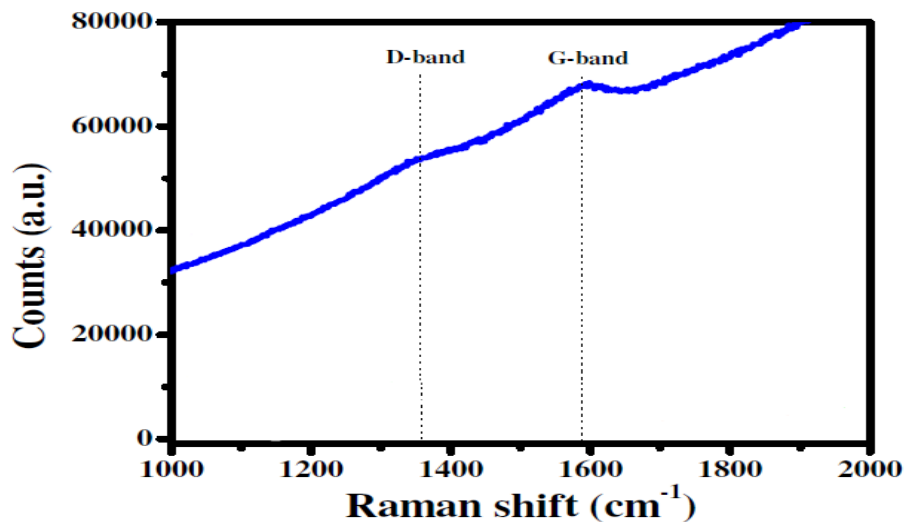


**Fig. 3.3.** Raman spectrum of C-dots after being exposed to a temperature of 300°C. Acquired from reference<sup>3</sup>.

The Raman spectrum of these C-dots show two peaks that dominate the spectra at approximately  $1595\text{ cm}^{-1}$  and  $1355\text{ cm}^{-1}$ , which can be labelled as the G and D bands respectively of the carbon that is amorphous (shown in **Fig 3.3**). The graphite lattice has a signature of disorder, which is thought to be responsible for the D peak. The  $\text{sp}^2$  bonded carbon has an  $\text{E}_{2g}$  vibration mode, which is responsible for the G peak.

### 3.2 Fluorescence Properties of Carbogenic Nanoparticles

After being exposed to UV light at wavelength 365 nm, images were taken of the Pluronic® P-123 32.5% w/t hydrogel with aC-dots. The same protocol was done for diluted solutions (0.05 mg/ml) of aC-dots and C-dots that were functionalised with JEFFAMINES® D-230 and D-400 respectively, as shown below (**Fig. 3.4**).



**Fig. 3.4.** Images of the fluorescence characteristics of 32.5% w/t P-123 hydrogel samples with aC-dots, and dilute solutions of aC-dots, JD-230 C-dots and JD-400 C-dots respectively from left to right. The hydrogel was made at a concentration of 0.103 mg/ml and each dilute solution was maintained at 0.05 mg/ml.

Carbogenic nanoparticles have great fluorescence properties, especially with regards to the aC-dots as shown above. Using the standard methods of preparation available to synthesise C-dots usually result in a very strong UV absorption peak. However, using different methods of preparation change these absorption peaks slightly, albeit still in the UV region. Using various

methods of preparation, C-dots of varying sizes have been synthesised with differing fluorescence characteristics:

Fluorescent C-dots that were synthesised by Dong *et al.* at 200°C via citric acid carbonisation. These nanoparticles were observed to see diameters of 15 nm, and when analysed with a UV-Vis spectrophotometer, they exhibited a thin peak at 362 nm. It was also observed that when the C-dots were exposed to various excitation wavelengths, it did not change the highest emission level<sup>145</sup>.

On the other hand, fluorescence C-dots that were water-soluble were prepared by sonicating a mixture of 70 mL hydrogen peroxide and 4.0 g of active carbon for 2 hours at approximately room temperature by Li *et al.* These nanoparticles were observed to see a diameter range of 5-10 nm, exhibiting a UV-Vis band peak at 250 – 300 nm showing the absorption of an aromatic pi system<sup>146</sup>.

With the use of a simple solvothermal technique, Jiang *et al.* exposed three types of C-dots to UV light at single excitation wavelengths, producing blue, green and red fluorescence. It was established that the photostability of all the C-dots in ethanol was good, but when the nanoparticles were exposed for an hour to UV light at wavelength 365 nm, the photostability was slightly decreased (by < 5%)<sup>147</sup>.

C-dots that were synthesised by Wang *et al.* involved vigorously mixing N-(β-aminoethyl)-γ-aminopropylmethyldimethoxysilane (AEAPMS) solution with half a gram of citric acid for 60 seconds at 240°C. The nanoparticles that were synthesised had an average diameter of 0.9 nm and upon analysed using UV-Vis they exhibited an intense absorption peak at 360 nm<sup>148</sup>.

### 3.2.1 Fluorescence Spectra of Carbogenic Nanoparticles

With excitation wavelengths ranging from 300 – 500 nm in the solid-like state fluorescence, it is clear that the strongest levels of fluorescence are from the excitation wavelengths that are in the UV region, with the maximum intensity being at 380 nm excitation. The emission wavelength peaks do not shift significantly with the change of excitation wavelength, showing the presence of fluorophores because they fluoresce independently of excitation wavelength (shown in **Fig. 3.5**). The aC-dots solution was made up to a concentration of 0.103 mg/ml because this was necessary to be able to see significant enough peaks in the fluorescence spectra.

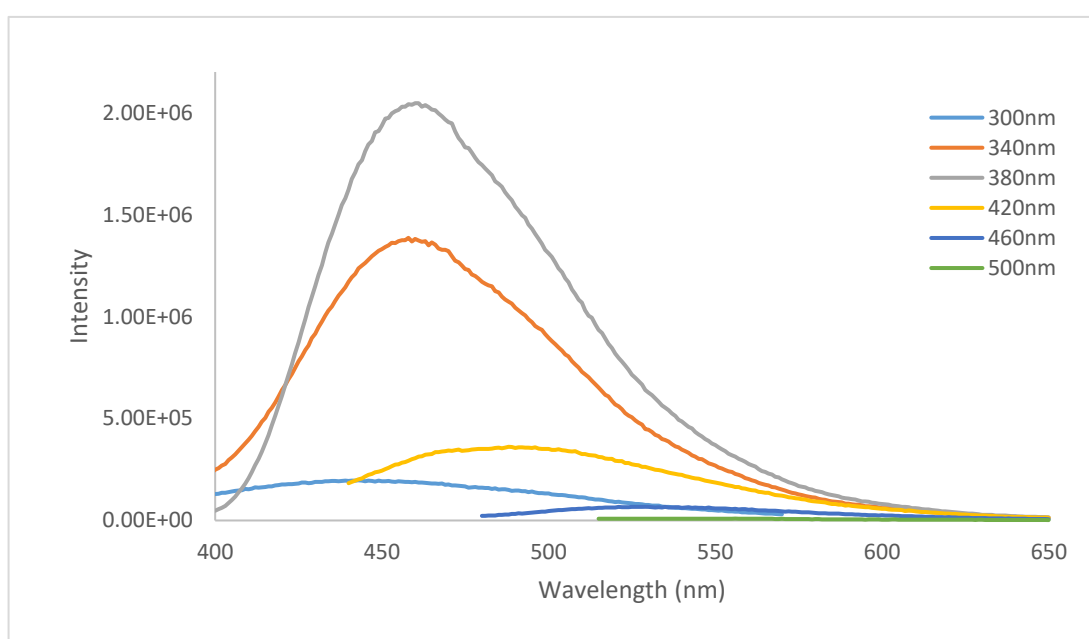


**Fig. 3.5.** Solid state fluorescence spectra of Pluronic® P-123 32.5% w/t hydrogel with 0.103 mg/ml aC-dots at excitation wavelengths 300, 340, 380, 420, 460 and 500 nm.

Kelarakis *et al.* used the same protocol of C-dot preparation to analyse the fluorescence levels of these C-dots at various temperatures (180, 230 and 300°C) and at excitation wavelengths ranging from 275 to 600 nm, increasing in 25 nm increments. Solutions were maintained at 0.1 mg/ml and it was found that the maximum intensity was observed for the excitation wavelength of 375 nm for the C-dots at 180°C and 230°C. This was not the case for the C-dots at 300°C

because at this temperature, the fluorescence comes from predominantly the carbogenic cores that form at higher temperatures, and the fluorescence levels are no longer dominated by the fluorophores. At this temperature, the highest intensity level was observed at an excitation wavelength of 275 nm<sup>8</sup>. The solid-like state fluorescence spectra above was done at room temperature, resulting in fluorophores being a significant contribution to the levels of fluorescence.

In liquid state fluorescence, the maximum emission intensity of the dilute solution of aC-dots is very similar the 32.5% w/t Pluronic<sup>®</sup> gel with aC-dots spectra. However, the concentration of the aC-dots in the liquid state fluorescence is half that of the solid state fluorescence.

In the C-dots solution it is much easier for the nanoparticles to aggregate together when compared to the C-dots in the Pluronic<sup>®</sup> gel. This is because the gel acts as a significant enough separating agent to keep the nanoparticles apart, stopping them from aggregating, thus maintaining good dispersion. This aggregation of nanoparticles in the C-dots solution creates clusters of C-dots, resulting in a poor dispersion of the C-dots, therefore potentially decreasing fluorescence emission intensity.

With the 0.05 mg/ml solution of aC-dots in water, the maximum emission intensity peaks at different excitations have not changed position for excitation wavelengths 320, 350, 380 and 410 nm. This suggest the presence of  $\lambda_{ex}$  independent fluorophores. All of the fluorescence emission peaks appear to have red-shifted somewhat.

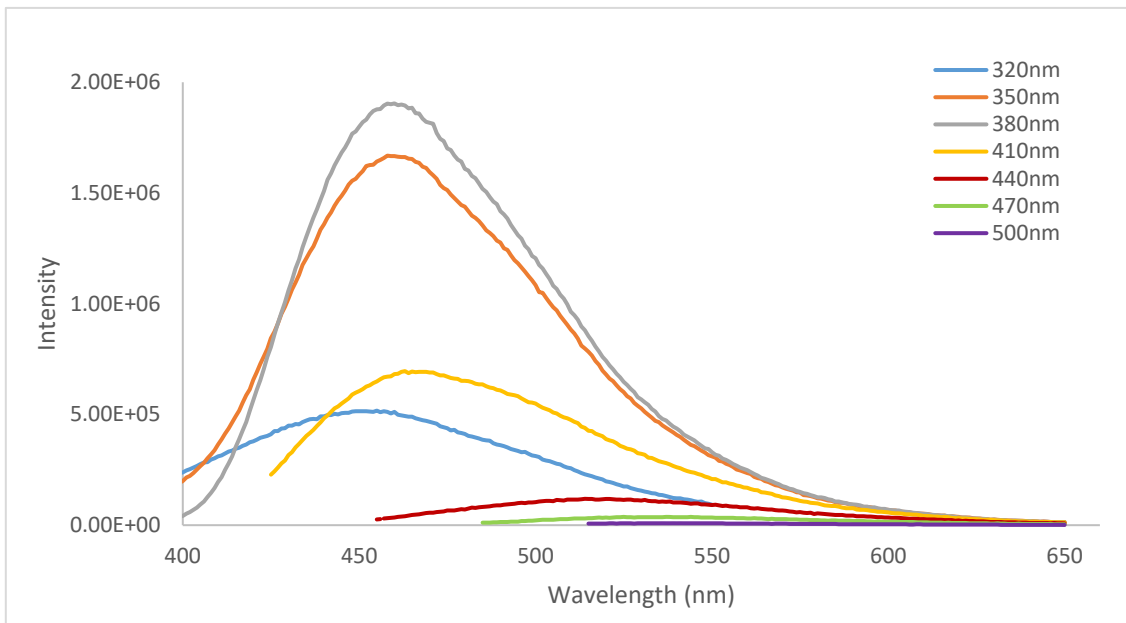


**Fig. 3.6.** Liquid state fluorescence spectra of a 0.05 mg/ml solution of aC-dots with water at excitation wavelengths 320, 350, 380, 410, 440, 470 and 500 nm.

The C-dots that were functionalised with JEFFAMINES® D-230 and D-400 were also analysed using liquid state fluorescence spectroscopy. The JD-230 and JD-400 C-dots showed similar spectra plots to each other, which is to be expected as they have the same fundamental structure with different molecular weights. These types of C-dots exhibited significantly lower intensity levels when compared to the aC-dots.

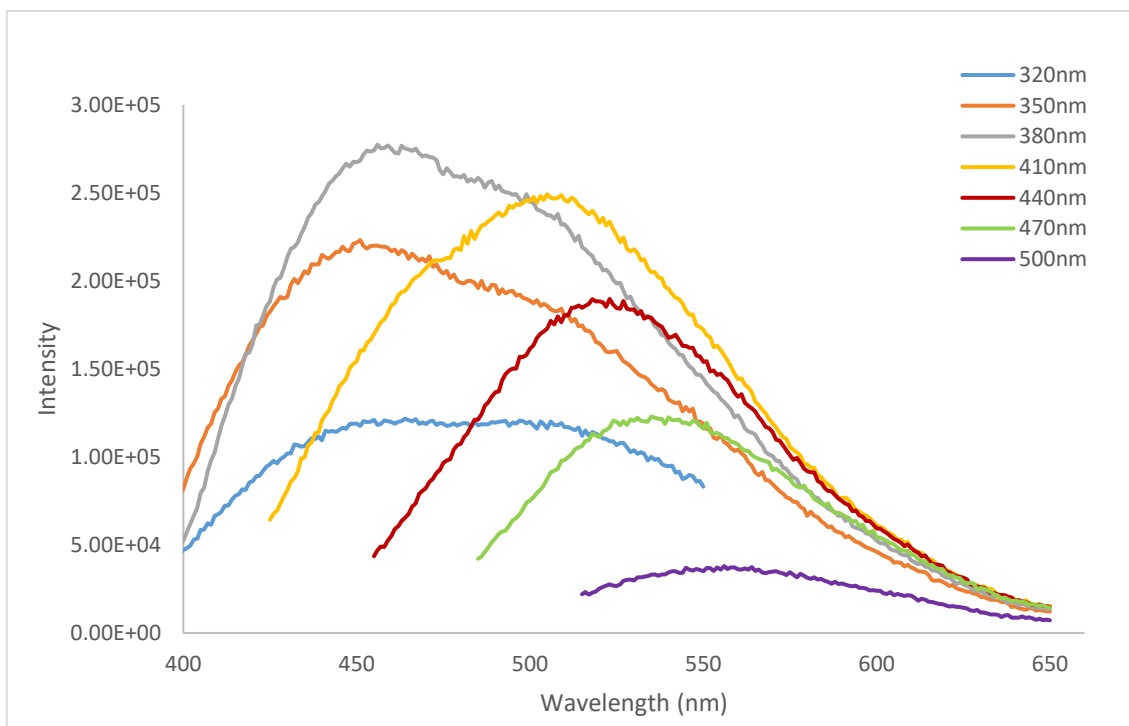


**Fig. 3.7.** Liquid state fluorescence spectra of a 0.05 mg/ml solution of JD-230 C-dots and water at excitation wavelengths 320, 350, 380, 410, 440, 470 and 500 nm.

This suggests a decrease in the amount of fluorophores present in the solution, which is supported when looking at the fact that the emission peaks in the C-dots functionalised with JEFFAMINES® are shifting as the excitation wavelengths change. Fluorophores fluoresce at the same wavelength regardless of the excitation wavelength, making them  $\lambda_{ex}$  independent. The shifting of maximum intensity peaks with changing excitation wavelengths shows the decrease in fluorophore levels, meaning the fluorescence is caused primarily by the C-dots which are  $\lambda_{ex}$  dependent.

The liquid state fluorescence of JD-400 C-dots shows a further decrease in maximum intensity levels when compared to the JD-230 C-dots. This suggests the possibility that the increasing size of the particles can decrease the amount of space available for the fluorescent C-dots when using equal quantities of each type of C-dot with the Pluronic® 32.5 wt% P-123 gels. In addition, although the amino groups that are present on the JEFFAMINES® have been established to improve fluorescence levels, there are only two amino groups on each JEFFAMINE® molecule. This further suggests that as the polymer size increases, the ratio of amino groups to the size of the chain decreases, therefore decreasing the effectiveness of the improved fluorescence levels that the amino groups can potentially provide.

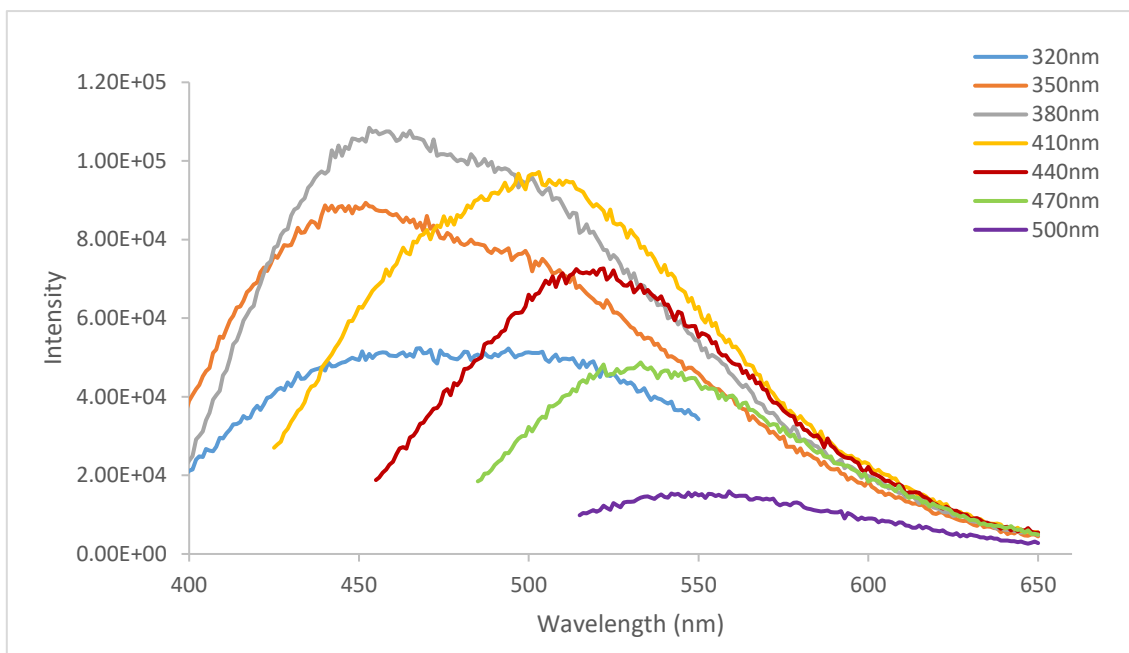


**Fig. 3.8.** Liquid state fluorescence spectra of a 0.05 mg/ml solution of JD-400 C-dots and water at excitation wavelengths 320, 350, 380, 410, 440, 470 and 500 nm.

With the fluorescence intensity peaks shifting position with the changes in excitation wavelength, this further supports the presence of primarily excitation dependent fluorescent carbogenic cores. The magnitude of shift in the maximum intensity peaks is almost identical to that of the JD-230 because they are of the same structures, but with different molecular mass.

In comparison, a study conducted by Wang *et al.* involved experiments on C-dots that were synthesised using JEFFAMINES® T-3000 and T-5000 as a carbon source, without a passivation agent. After 15 heating-cooling cycles for 45 min each in a 300W microwave, the organic compound changed from a transparent to a dark brown solution. Upon the addition of 1 mL of deionised water to this solution, the C-dots were extracted via the use of a centrifuge. Finally, the C-dots were well dispersed in an aqueous supernatant that was golden-yellow in colour. These two types of C-dots were exposed to UV-light to display a blue fluorescence, showing emission peaks that were centred at 448 nm and 439 nm for the JT-3000 and JT-5000 C-dots respectively. The maximum intensity peaks had a broad range in the visible light spectrum,

varying from 400 nm to 500 nm with a range of excitation wavelengths from 325 nm to 405 nm. In this experiment, it was established that the JT-3000 and JT-5000 C-dots had a photoluminescence that was  $\lambda_{\text{ex}}$  dependent<sup>149</sup>.

### 3.2.2 Fluorescence Microscopy Images

Using a Zeiss Axio Scope A1 microscope with band pass filters, sample vials of water, aC-dots, JD-230 C-dots and JD-400 C-dots were exposed to three excitation wavelengths (350, 395 and 590 nm respectively) and these fluorescence microscopy images were obtained. The light pathways through the samples were observed and fluorescence properties were compared. As a standard, these characteristics were compared with the light pathways through water.

The fluorescence microscopy images of aC-dots, JD-230 C-dots and JD-400 C-dots when exposed to light at wavelengths 350, 395 and 500 nm (respectively from top to bottom) clearly show distinct light pathways through the C-dot solutions in comparison to water, as shown in **(Fig. 3.9)**. The first thing to be noticed is that when the aC-dots were exposed to light at wavelength 350 nm (Ultraviolet), they fluoresce a darker blue compared to the C-dots functionalised with JEFFAMINES® fluorescing light-blue/white.

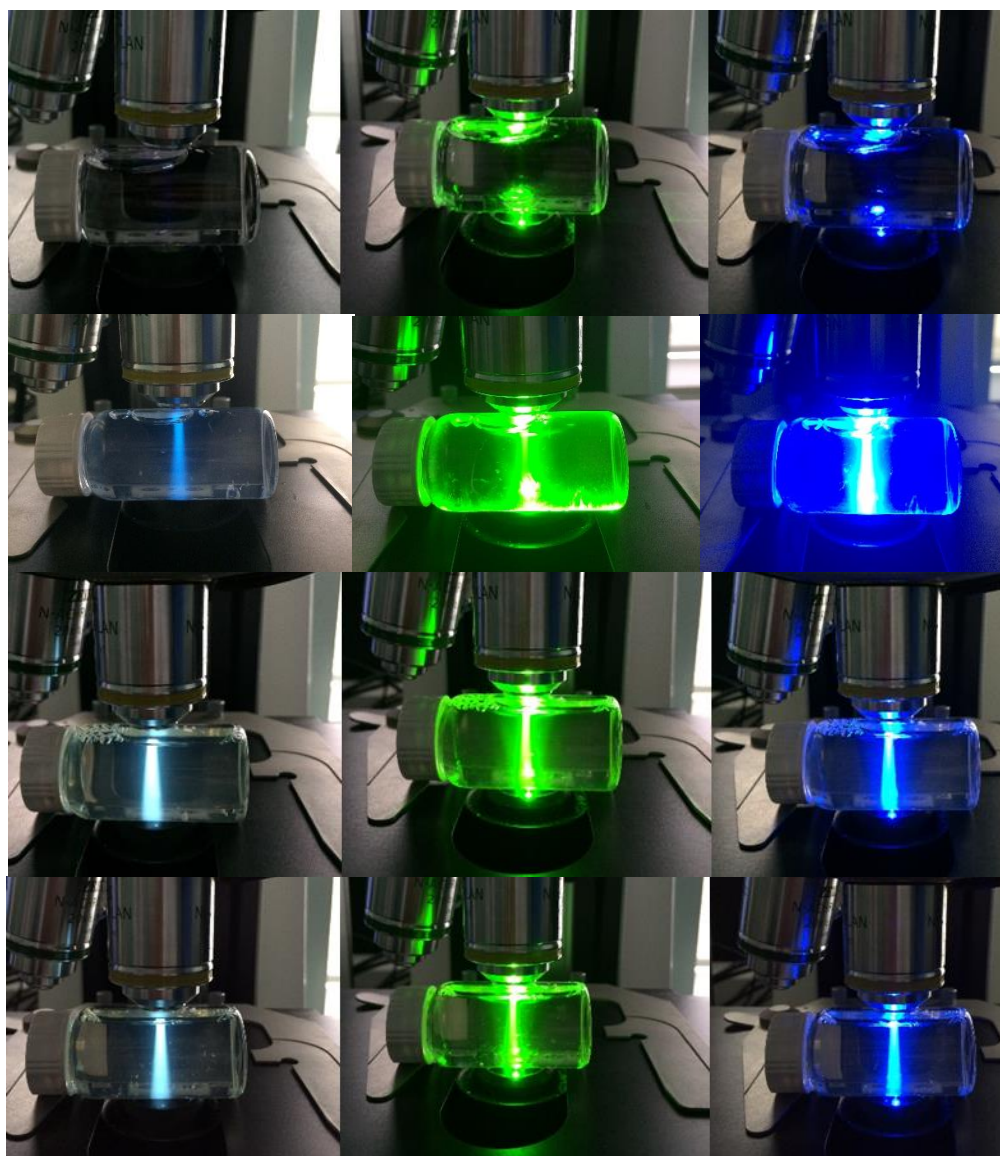


**Fig. 3.9.** Fluorescence microscopy images of sample vials with water, aC-dots, JD-230 C-dots and JD-400 C-Dots when exposed to light at wavelengths 350, 395 and 590 nm using a fluorescence microscope with band-pass filters. The top row of images show water, 2<sup>nd</sup> row aC-dots, 3<sup>rd</sup> row JD-230 C-dots, and bottom row JD-400 C-dots.

This is supported by the fluorescence spectra of these C-dots (see **Fig. 3.6, 3.7 and 3.8**), showing that the maximum intensity peaks of the JD-230 and JD-400 C-dots at excitation wavelength 350 nm have shifted to the left, more towards the UV region of the spectrum. In addition, the fluorescence intensity of the aC-dots when exposed to light at wavelength 395 nm (Green) is significantly higher than that of the C-dots functionalised with JEFFAMINES<sup>®</sup>. This can be supported by looking at the maximum intensity peaks on the fluorescence spectra at excitation

wavelengths 380 and 410 nm, both of which have significantly higher emission intensities in aC-dots than the JD-230 and JD-400 C-dots.

A study lead by Baker *et al.* involved C-dots that were synthesised by a one-step laser passivation method. It was shown that C-dots that were synthesised by laser ablation only exhibited fluorescence emission upon being surface passivated by specific organic moieties, whether in solid state or dispersed in solution. Therefore, the C-dots were in aqueous solution and were passivated with PEG<sub>1500N</sub>. The C-dots were excited at 400 nm with images taken through band-pass filters of wavelengths 400, 450, 500, 550, 600, 650 and 690 nm. Images were also taken directly upon the excitation of the C-dots at the same wavelengths. The C-dots in this study exhibited a strong  $\lambda_{\text{ex}}$  dependence, resulting in the emission peaks red shifting with increases in excitation wavelength<sup>26</sup>. This strong dependence on  $\lambda_{\text{ex}}$  does concur with the fluorescence images and spectra in this project. However, the colour-shift occurred in the opposite direction, showing the widely contrasting fluorescence behaviours of different types of C-dots.

### 3.3 Gel Phase Behaviour

To determine the gel phase behaviours of 32.5 wt% Pluronic® P-123 hydrogels with the presence of different types of C-dots, the gels were heated from 5°C to 75°C to establish the temperatures at which the sol-gel (lower) and gel-sol (upper) transitions occur. These transitions were determined for P-123 hydrogels with JD-230 C-dots and JD-400 C-dots, aC-dots and without C-dots (shown in **Fig 3.10**).

The JD-230 C-dots and aC-dots did not affect the sol-gel transition temperature, but the JD-400 did affect it significantly, reducing it by 10°C. However, the gel-sol transition temperature varied depending on the type of C-dots that were present, with all types of C-dots increasing the

temperature by different amounts. With the gel-sol transition temperature of P-123 32.5 wt% hydrogel starting at 62°C, the aC-dots, JD-400 C-dots and JD-230 C-dots increased this transition temperature by 2°C, 4°C and 6°C respectively. In other words, the incorporation of C-dots does not compromise the highly desirable injectable nature of the Pluronic® gels, given that the C-dot based gels also exhibit a sol-gel transition below body temperature. This behaviour can in principle allow the injection of a sol system (avoiding the need for a surgical treatment) that instantly becomes immobile to the home body, offering localised and targeted treatment.

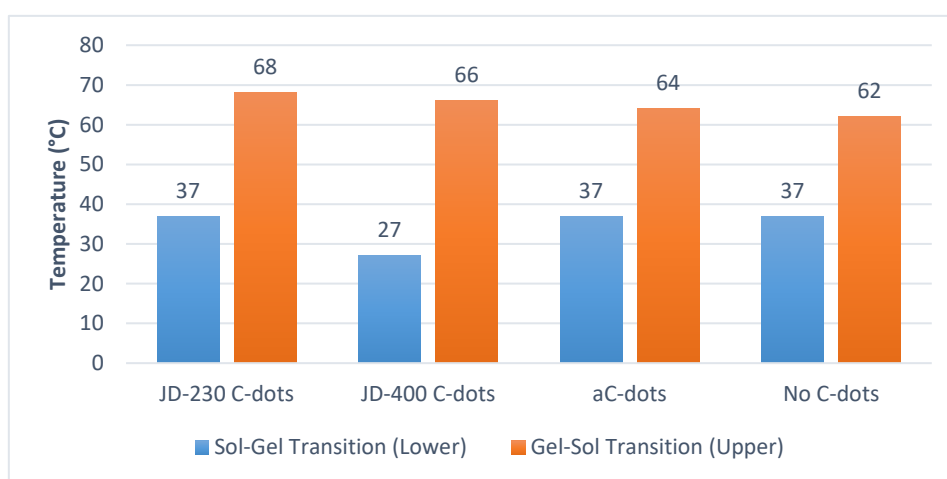


**Fig 3.10.** Gel phase behaviours of 32.5% w/t P-123 hydrogels with the presence of various types of C-dots and without any C-dots, shown in the form of a histogram.

A study led by Jeong *et al.* confirmed that the sol-gel and gel-sol transitions are influenced significantly by the concentration of polymer present. The method they used yielded the phase transition temperatures of Pluronic® gels to an accuracy of  $\pm 0.5^\circ\text{C}$ . For the lower sol-gel transition, this was done with gel concentrations of 17 - 40 wt% that were exposed to a gradual temperature decrease to 30°C from 36°C. It was shown that this transition was highly concentration dependent. For the upper gel-sol transitions, the same varying concentrations of polymer gels were subjected to increasing temperature from 44°C to 70°C, also revealing that the transition temperatures were concentration dependent<sup>99</sup>.

## 3.4 Drug Release Studies

### 3.4.1 Ibuprofen Calibration Curve

To begin studying the release rates of IBU in Pluronic® P-123 hydrogels with the presence of various types of C-dots, an IBU calibration curve must be plotted to do calculations against later. The calibration curve was done by preparing samples of IBU in increasing concentrations of 0.01, 0.03, 0.05, 0.09, 0.1, 0.3, 0.5, 0.7 and 0.9 mg/ml in a buffer solution of citric acid and sodium phosphate dibasic at a pH of 7.4. UV-vis spectroscopy indicated that the maximum absorbance occurs at 263 nm, in agreement with literature. Therefore, the absorbance at 263 nm was taken to plot the calibration curve (see **Methodology Section – Fig 2.1**).

Each gel had a total weight of 10g, with 50mg of IBU present in the mixture, meaning the standard concentration of IBU in each mixture was 0.5 wt%. This concentration of IBU was consistent throughout all gels, including those with the presence of aC-dots, JD-230 C-dots and JD-400 C-dots. The release profiles of IBU in all of these gels were observed at room temperature against 200mL of 1.0 M buffer solution at pH 7.4. Each process of dialysis was left for a long period of time with frequent samples taken to study the rate of release of IBU.

### 3.4.2 Release Profiles without C-dots

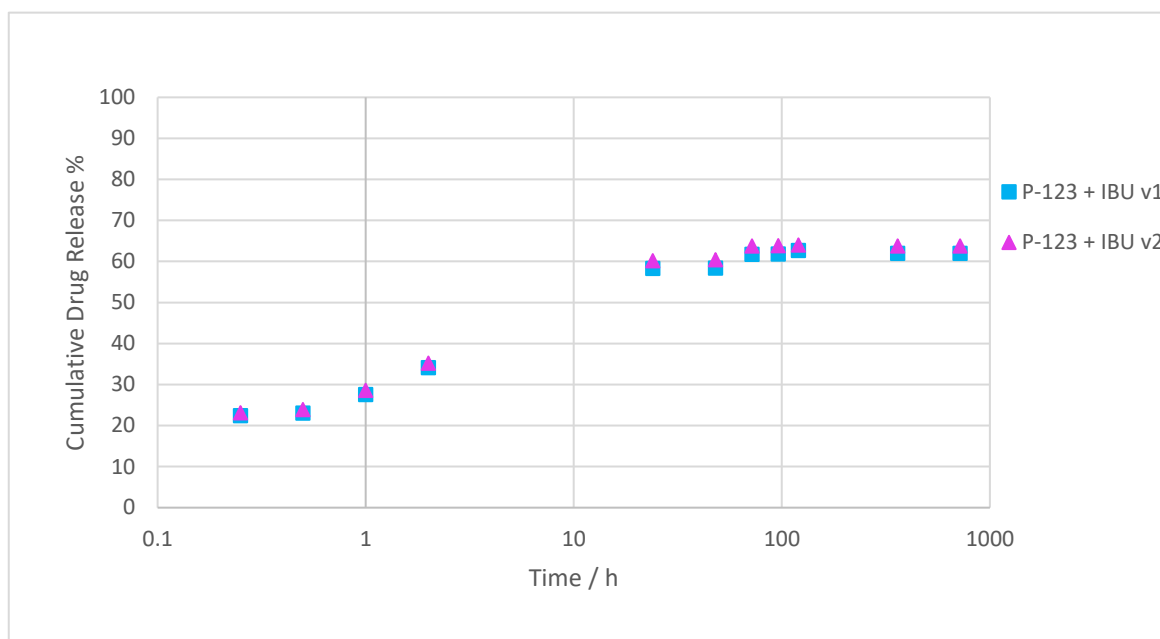


**Fig. 3.12.** Release profiles of Ibuprofen from Pluronic® P-123 hydrogels against a phosphate buffer solution (pH 7.4) at room temperature, without the presence of any C-dots.

In each mixture, regular samples were taken over a long enough period of time so that the IBU could reach the maximum release percentage achievable for that mixture. In this experiment, the polymer appears to remain inside of the dialysis tubing due to its molecular weight cut-off of 3.5 kDa, and the IBU had no issue passing through. There were a negligible amount of fluorophores that had passed through the tubing into the PBS 7.4 pH, because the solutions were the same colour before and after dialysis. Except with the C-dots functionalised with JEFFAMINES®, in which the buffer solution changed to a very pale yellow, almost clear.

In the various dialysis experiments, it is clear that the presence of C-dots and what type of C-dots they were, did significantly affect the IBU total release percentage and the rate at which IBU was released. With regards to the Pluronic® gel without any C-dots present, the drug appears to be burst released up to ≈35% within the first 3 hours and continues to be released rapidly, reaching a maximum release of 60-65% within 24 hours in both attempts (as shown in **Fig. 3.12**).

### 3.4.3 Release Profiles with C-dots

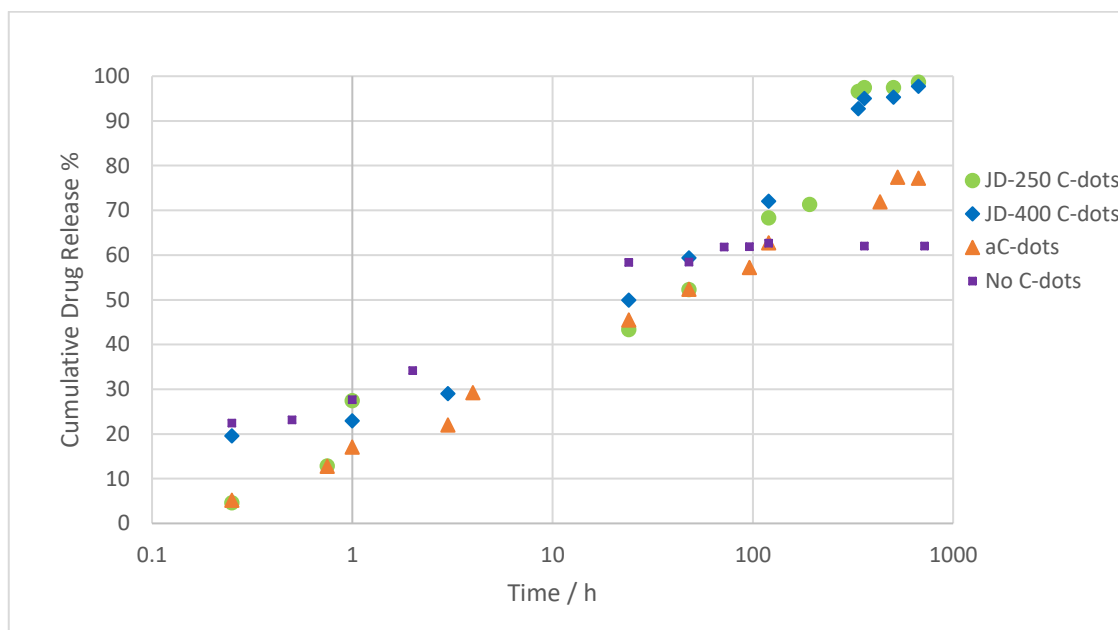


**Fig. 3.13.** *In vitro* release profiles of Ibuprofen from Pluronic® P-123 hydrogels against a phosphate buffer solution (pH 7.4) at room temperature. The squares represent the gel without the presence of any C-dots. The circles, diamonds and triangles represent the gels with JD-230 C-dots, JD-400 C-dots and aC-dots respectively.

The cumulative drug release percentages were calculated by taking the absorbance levels at 263 nm for Ibuprofen as the y value in  $(y = mx + c)$ , then rearranged to calculate x. This value was then multiplied by the total volume of solution outside of the dialysis tubing, then multiplied by 1000 to translate the decimals into percentages.

Looking at the release profiles of IBU in P-123 hydrogels with various C-dots (shown in **Fig. 3.13**), the drug release from the aC-dots and JD-230 C-dots indicate the most gradual rates of release. The aC-dots show a sustained rate of release throughout dialysis, gradually reaching 29% drug release within 24 hours, and reaching a maximum release of approximately 77%. The JD-230 exhibit a very similar trend, but reach a maximum release of  $\geq 95\%$  after about 2 weeks, showing an enhanced drug release in comparison to the gel with aC-dots. The gels with JD-400 exhibit

burst release at the start, up to 19.5% in the first 15 minutes, releasing about 30% within 24 hours, then a gradual release to reach a maximum drug release of  $\geq 95\%$  after 2 weeks.

It is clear that the maximum drug release percentage of the gels with C-dots functionalised with JEFFAMINES<sup>®</sup> is higher than that of the gels with aC-dots. This increase in release could be due to the release of the close packing constrains, along with the possibility of effective channels forming that can facilitate the diffusion of the drug out of the gels. These plots show that in Pluronic<sup>®</sup> hydrogels, the presence of different types of C-dots not only slows the rate of release down to a more controlled and sustained rate, but also allows the drug to reach a higher release percentage, showing enhanced drug release when compared to the Pluronic<sup>®</sup> hydrogels without C-dots. The most successful drug release profile appears to be that of the Pluronic<sup>®</sup> P-123 hydrogel with C-dots functionalised with JEFFAMINE<sup>®</sup> D-230, with the highest maximum drug release of indicating a slow and sustained rate of drug release through the dialysis tubing over the course of 4 weeks. In addition, this drug delivery system exhibited the most enhanced drug release due to its maximum drug release percentage being the highest.

A study conducted by Liu *et al.* showed experiments observing the release of Docetaxel (DTX) *in vitro*. With the use of Tween 80-free as a medium to improve the solubility of DTX, the drug was loaded into Pluronic<sup>®</sup> P-123. Using a dialysis bag with a molecular weight cut-off of 8-14 kDa, the drug was dialysed at 37°C against a buffer solution at pH 7.4. After 24 hours, the DTX reached 84.05% released. The drug was released via diffusion and dissolution from the DTX micelles, and it was established that the DTX delivery system was effectively influenced by the P-123 micelles<sup>150</sup>.

Similarly, experiments with similar parameters were conducted by Han *et al.* observing the *in vivo* and *in vitro* of paclitaxel (PTX) which was also loaded into Pluronic<sup>®</sup> P-123. Using the

method of solid dispersion, the drug was dispersed within the P-123, filtered and then freeze-dried. The remaining substance was then dissolved again into water, and 1mL of this solution was dialysed against 50mL of sodium salicylate at a concentration of 1 mol/L at 37°C for 24 hours. The dialysis tubing had a molecular weight cut-off of 5 kDa. Approximately 40% of the drug was released in the first 4 hours, and reached a maximum release percentage of 87.8% within 24 hours. Using this data, Pluronic® P-123 was shown to be an effective candidate for the carrying of insoluble drugs. It also increases the half-life of the drug by controlling the release delivery system<sup>151</sup>.

Alternatively, a research project led by Jeong *et al.* studies the drug release profiles of spironolactone and ketoprofen, which both had hydrophobic properties that were different. These drugs were release from PEG-PLGA-PEG triblock copolymer hydrogel formed *in situ* by injecting these solutions into aqueous environments at 37°C. It was shown that the ketoprofen had a first order release profile, exhibiting burst release up to 40% within the first 24 hours and reached a maximum drug release of about 90% within 1 week from the 33 wt% hydrogel. However, the spironolactone showed an S-shaped release profile, exhibiting an initial burst release up to 20% within about 24 hours, and then showed a slowly increasing rate of release up to about 70% after 55 days<sup>152</sup>.

### 3.4.4 Release Profiles of Paracetamol and Ibuprofen Compared

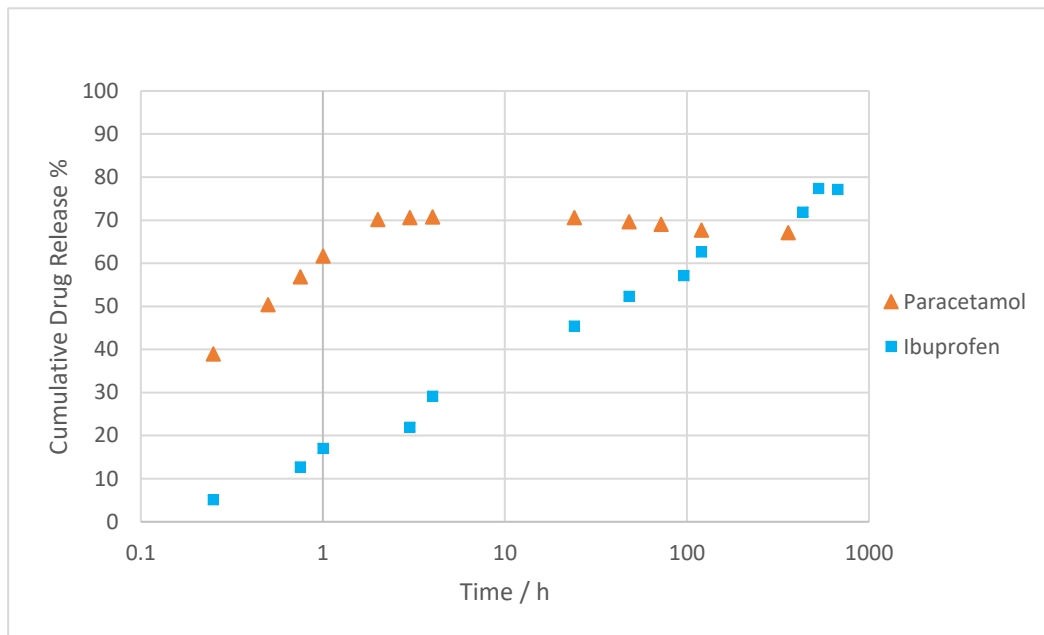


**Fig 3.14.** *In vitro* release profiles of PCL and IBU in P-123 hydrogel with the presence of aC-dots against a phosphate buffer solution (pH 7.4). The triangles represent the hydrogel with PCL, and the squares represent the hydrogel with ibuprofen.

Looking at the release profiles of PCL when compared to IBU from a P-123 hydrogel with the presence of aC-dots, it is clear that PCL follows a very different release pattern. Analysis shows that the drug burst released up to approximately 39% within the first 15 minutes, reaching a maximum drug release of 70% after two hours. The rate of release is significantly faster in the release profile of PCL when compared to that of IBU, but both reach a similar maximum release percentage. The fast release of PCL should be attributed to its hydrophilic nature that allows its dispersion directly into the aqueous medium, as opposed to IBU that resides to the micellar interior.

## 4. Conclusion

Currently, the amount of medicines involving nanotechnology is climbing, set to spread exponentially<sup>8</sup>. More specifically, with the vast potential of carbonogenic nanoparticles in the field of medicine becoming such a significant concept of focus for so many scientists, the pharmaceutical industry is beginning to change. The C-dots that were synthesised in this project via the pyrolysis at 300°C of ethanolamine and citric acid monohydrate exhibited fantastic fluorescence properties upon various excitation wavelengths, with the highest emission intensities occurring upon excitation with UV light at wavelength 350 nm. The fluorescence emission intensities of the C-dots were significantly reduced upon functionalisation with JEFFAMINES® D-230 and D-400, with intensity decreasing along with increasing polymer size. This could be attributed to the large polymer increasing the total size of the particles, reducing the ratio of fluorescent carbon cores that are present. The gel phase transition temperatures indicate that the addition of C-dots does not compromise the highly desirable injectable nature of the Pluronic® gel, since a sol-gel temperature was observed below the body temperature in all cases.

At the same time, the fluorescence spectra indicate a clear increase in  $\lambda_{ex}$  dependence for the C-dots functionalised with JEFFAMINES® in comparison to without. This characteristic shows promise in improved biological imaging, due to the improved penetration that Infra-red radiation has through living tissue.

The *in vitro* drug release profiles of IBU in 32.5 wt% Pluronic® P-123 hydrogels with and without various types of C-dots showed that the drug release was enhanced with the presence of all types of C-dots. The release profiles that were most significantly enhanced could be seen for the 32.5% wt p-123 with JD-230 and JD-400 C-dots. Both reached a maximum drug release of above 95%, over a very long period of time (about 2 weeks) when dialysed at room temperature against a phosphate buffer solution (pH 7.4). Overall, the IBU drug release profile of the P-123

hydrogel with JD-230 showed the most enhanced drug release with a controlled and sustained release up to a maximum release of over 95%. The release profiles indicate an increase in maximum drug release with the presence of C-dots, showing the possibility of released of close packing constrains, allowing the drug to diffuse out of the gel more efficiently. In addition, the gels with C-dots have the potential to facilitate the diffusion of the drug by creating efficient channels.

Future work to be done on carbogenic nanoparticles and their biomedical applications include deeper investigation into the drastically contrasting release profiles of ibuprofen and PCL when loaded into thermo-reversible Pluronic® gels with aC-dots. The release profiles of many different types of therapeutic drugs must be taken into experimentation to further understand the increasing potential of C-dots.

To that end, the present work contributes significant evidence that C-dots are promising materials for the development of novel theragnostics, allowing simultaneous monitoring of the cells, while offering an additional level of drug release control.

## References

1. Kellarakis. A, *MRS. Energy and Sustainability*, 2014, **1**, p. 1
2. Krysmann. M. J, Kellarakis. A, Giannelis. E. P, *Green Chem.*, 2012, **14**, p. 3141
3. Krysmann. M. J, Kellarakis. A, Dallas. P, Giannelis. E. P, *J. Am. Chem. Soc.*, 2012, **134**, p. 747
4. Desmonts. L. B, Reinhoudt. D. N, Calama. M. C, *Chem. Soc. Rev.*, 2007, **36**, p. 993
5. Colton R. J, Russell J. N, *Science*, 2003, **299**, p. 1324
6. Yang J. S, Swager T. M, *J. Am. Chem. Soc.*, 1998, **120**, p. 11864
7. Xu. X, Ray. R, Gu. Y, Ploehn. H. J, Gearheart. L, Raker K., Scrivens W. A, *J. Am. Chem. Soc.*, **2004**, 126, p. 12736
8. Tao. H, Yang. K, Ma. Z, Wan. J, Zhang. Y, Kang. Z, Liu. Z, *Small*, 2012, **8**, p. 281
9. Zhao. A, Chen. Z, Zhao. C, Gao. N, Ren. J, Qu. X, *Carbon*, 2015, **85**, p. 309
10. Pandey. S, Mewada. A, Thakur. M, Tank. A, Sharon. M, *RSC Adv.*, 2013a, **3**, p. 26290
11. Suna. W, Dua. Y, Wangd. Y, *J. Luminescence*, 2010, **130**, p. 1463
12. Zhu. S, Song. Y, Zhao. X, Shao. J, Zhang. J, Yang. B, 2015, *Nano. Research*, **8**, p. 355
13. Li. H, Kang. Z, Liu. Y, Lee. S, *J. Mater. Chem*, 2012, **22**, p. 24230
14. Baker. S, Baker. G, *Ang. Chem. Int. Ed.*, 2010, **49**, p. 6726
15. Zhai. X, Zhang. P, Liu. C, Bai. T, Li. W, Dai. L, Liu. W, *Chem. Comm.*, 2012, **48**, p. 7955
16. Wei. W, Xu. C, Wu. L, Wang. J, Ren. J, Qu. X, *Sci. Rep.*, 2014, **4**, p. 3564
17. Xu. Y, Ray. R, Gu. Y, Ploehn. H, Gearheart. L, Raker. K, Scrivens. W, *Chem. Euro. J.*, 2013, **19**, p. 12736
18. Qian. Z, Ma. J, Shan. X, Feng. H, Shao. L, Chen. J, *Chem. Euro. J.*, 2014, **20**, p. 2983
19. Kwon. W, Lim. J, Lee. J, Park. T, Rhee. S, *J. Mat. Chem.*, 2013, **1**, p. 2002
20. Jiang. J, He. Y, Li. S, Cui. H, *Chem. Comm.*, 2012, **48**, p. 9634
21. Dong. Y, Pang. H, Yang. H. B, Guo. C, Shao. J, Chi. Y, Li. C. M, Yu. T, *Ang. Chem. Int. Ed.*, 2013, **52**, p. 7800
22. Dong. Y, Wang. R, Li. H, Shao. J, Chi. Y, Lin. X, Chen. G, *Carbon*, 2012b, **50**, p. 2810
23. Chandra. S, Patra. P, Pathan. S. H, Roy. S, Mitra. S, Layek. A, Bhar. R, Pramanik. P, Goswami. A, *J. Mat. Chem. B*, 2013, **1**, p. 2375
24. Wang. X, Cao. L, Yang. S, Lu. F, Meziani. M. J, Tian. L, Sun. K. W, Bloodgood. M. A, Sun. Y, *Ang. Chem. Int. Ed.*, 2010, **49**, p. 5310
25. Hu. S. L, Niu. K. Y, Sun. J, Yang. J, Zhao. N. Q, Du. X. W, *J. Mater. Chem.*, 2009, **19**, p. 484
26. Baker. S. N, Baker. G. A, *Angew. Chem. Int. Ed.*, 2010, **49**, p. 6726
27. Fang. Y, Guo. S, Li. D, Zhu. C, Ren. W, Dong. S, Wang. E, *ACS. Nano.*, 2011, **6**, p. 400
28. Baker. S. N, Baker. G. A, *Angew. Chem. Int. Ed.*, 2010, **49**, p. 6726
29. Mao. X. J, Zheng. H. Z, Long. Y. J, Du. J, Hao. J. Y, Wang. L. L, Zhou. D. B, *Spectrochim. Acta.*, 2009, **75**, p. 553

30. Bourlinos. A. B, Zbořil. R, Petr. J, Bakandritsos. A, Krysmann. M, Giannelis. E. P, *Chem. Mater.*, 2011, **24**, p. 6
31. Chien. C. T, Li. S. S, Lai. W. J, Yeh. Y. C, Chen. H. A, Chen. I. S, Chen. L. C, Chen. K. H, Nemoto. T, Isoda. S, Chen. M, Fujita. T, Eda. G, Yamaguchi. H, Chhowalla. M, Chen. C. W, *Angew. Chem. Int. Ed.*, 2012, **51**, p. 6662
32. Díaz. M. R, Vivas-Mejia. P. E, *Pharmaceuticals*, 2013, **6**, p. 1365
33. Cao. L, Wang. X, Mezziani. M. J, Lu. F, Wang. H, Luo. P. G, Lin. Y, Harruff. B. A, Veca. L. M, Murray. D, *J. Am. Chem. Soc.*, 2007, **129**, p. 11318
34. Yang. S. T, Wang. X, Wang. H, Lu. F, Luo. P. G, Cao. L, Mezziani. M. J, Liu. J. H, Liu. Y, Chen. M, *J. Phys. Chem. C.*, 2009, **113**, p. 18110
35. Yang. S. T, Cao. L, Luo. P. G, Lu. F, Wang. X, Wang. H, Mezziani. M. J, Liu. Y, Qi. G, Sun. Y. P, *J. Am. Chem. Soc.*, 2009, **131**, p. 11308
36. Tao. H, Yang. K, Ma. Z, Wan. J, Zhang. Y, Kang. Z, Liu. Z, *Small*, 2012, **8**, p. 281
37. Sun. Y. P, Zhou. B, Lin. Y, Wang. W, Fernando. K. A, Pathak. P, Mezziani. M. J, Harruff. B. A, Wang. X, Wang. H, Luo. P. G, Yang. H, Kose. M. E, Chen. B, Veca. L. M, Xie. S. Y, *J. Am. Chem. Soc.*, 2006, **128**, p. 7756
38. Sun. Y. P, Wang. X, Lu. F, Cao. L, Mezziani. M. J, Luo. P. G, Gu. L, Veca. L. M, *J. Phys. Chem. C*, 2008, **112**, p. 18295
39. Wang. J, Zhang. P, Huang. C, Liu. G, Leung. K. C. F, Wang. Y. X. J, *Langmuir*, 2015, **31**, p. 8063
40. Tao. H, Kai. Y, Ma. Z, Wan. J, Zhang. Y, Kang. Z, Liu. Z, *Small*, 2012, **8**, p. 281
41. Zeng. Q, Shao. D, He. X, Ren. Z, Ji. W, Shan. C, Qu. S, Li. J, Chen. L, Li. Q, *J. Mater. Chem. B*, 2016, **4**, p. 5119
42. Feng. T, Ai. X, Ong. H, Zhao. Y, *Appl. Mater. Interfaces*, 2016, **8**, p. 18732
43. Karthik. S, Saha. B, Ghosh. S. K, Singh. N. D. P, *Chem. Commun.*, 2013, **49**, p. 10471
44. Zawilska. J. B, Wojcieszak. J, Olejniczak. A. B, *Institute Of Pharmacology*, 2013, **65**, p. 1
45. Rautio. J, Kumpulainen. H, Heimbach. T, Oliyai. R, Oh. D, Järvinen. T, Savolainen. J, *Nat. Rev. Drug. Discov.*, 2008, **7**, p. 255
46. Azori. M, *Crit. Rev. Ther. Drug. Carrier. Syst.*, 1987, **1**, p. 39
47. Huttunen. K. M, Raunio. H, Rautio. J, *Pharmacol. Rev.*, 2011, **3**, p. 750
48. Stella. V. J, *J. Pharm. Sci.*, 2010, **99**, p. 4755
49. Testa. B, *Curr. Opin. Chem. Bio.*, 2009, **13**, p. 338
50. Li. M, Liang. Z, Sun. X, Gong. T, Zhang. Z, 2014, *J. PLOS*, **10**, p. 1371
51. Ulbrich. K, Subr. V, Strohalm. J, Plocová. D, Jelínková. M, *J. Control. Release*, 2000, **64**, p. 63
52. Ringsdorf. H, *J. Polym. Sci. Symp*, 1975, **51**, p. 135

53. Allen. T. M, *Nat. Rev. Cancer*, 2002, **2**, p. 750
54. Etrych. T, Chytil. P, Jelinkova. M, Rihova. B, Ulbrich. K, *Macromol. Biosci*, 2002, **2**, p. 43
55. Duncan. R, Robinson. J. R, Lee. V. H. L, *Marcel. Dekker*, 1987, **1**, p. 581
56. Vassalli. J. D, Pepper. M.S, *Tum. Bio.*, 1994, **370**, p. 14
57. Jatzkewitz. H. Z, *Naturf.*, 1955, **10b**, p. 27
58. Thistlethwaite. A. J, Leeper. D.B, Moylan. D.J. 3rd, Nerlinger. R.E, *Int. J. Radiat. Oncol. Biol. Phys.*, 1985, **11**, p. 1647
59. Kratz. F, Beyer. U, Schütte. M. T, *Crit. Rev. Ther. Drug. Carrier. Syst.*, 1999, **16**, p.245
60. Matsumura. Y, Maeda. H, *Cancer. Res*, 1986, **46**, p. 6387
61. Mego. J. L, McQueen. J. D, *Cancer. Res*, 1965, **25**, p. 865
62. Yancopoulos. G. D, Klagsbrun. M, Folkman. J, *Cell*, 1998, **93**, p. 661
63. Maeda. M, Izuno. Y, Kawasaki. K, Kaneda. Y, Mu. Y, *Chem. Pharm. Bull*, 1997, **45**, p. 1788
64. Goldstein. I. J, Hugues. R. C, Monsigny. M, Osawa. T, Sharon. N, *Nature*, 1980, **285**, p. 65
65. Maeda. H, Wu. J, Sawa. T, Matsumura. Y, Hori. K, *J. Control. Release*, 2000, **65**, p. 271
66. Maeda. H, *Adv. Drug. Deliv. Rev*, 2001, **46**, p. 169
67. Seymour. L.W, Miyamoto. Y, Maeda. H, Brereton. M, Strohalm. J, *Eur. J. Cancer*, 1995, **31A**, p. 766
68. Maher. S, Toomey. D, Condrón. C, Bouchier-Hayes. D, *Immunol. Cell. Biol*, 2002, **80**, p. 131
69. Coessens. V, Schacht. E, Domurado. D, *J. Control. Release*, 1996, **38**, p. 141
70. Krammer. P.H, Dhein. J, Walczak. H, Behrmann. I, Mariani. S, *Immunol. Rev*, 1994, **142**, p. 175
71. Amulya. K, *J. Thoracic. Cardiovasc. Surg.*, 2010, **139**, p. 496
72. Wang. F, Li. Z, Khan. M, Tamama. K, Kuppusamy. P, *Acta. Biomater.*, 2010, **6**, p. 1978
73. Kashyap. N, Kumar. N, Kumar. M, *Crit. Rev. Ther. Drug. Carr. Syst.*, 2005, **22**, p. 107
74. Zhang. L, Li. K, Xiao. W, Zheng. L, Xiao. Y, Fan. H, *Carbohydr. Polym.*, 2011, **84**, p. 118
75. Van der Linden. H. J, Herber. S, Olthius. W, Bergveld. P, *Analyst*, 2003, **128**, p. 325
76. Kaihara. S, Matsumara. S, Fisher. J. P, *Eur. J. Pharm. Biopharm.*, 2008, **68**, p. 67
77. Krsko. P, McCann. T. E, Thach. T. T, Laabs. T. L, Geller. H. M, Libera. M. R, *Biomat.*, 2009, **30**, p. 721
78. Sikareepaisan. P, Ruktanonchai. U, Supaphol. P, *Carbohydr. Polym.*, 2011, **83**, p. 1457
79. Anisha. S, Kumar. S. P, Kumar. G. V, Garima. G, *Hydrogels*, 2010, **1**, p. 1
80. Roy. D, Cambre. J. N, Brent. S, *Prog. Polym. Sci.*, 2010, **35**, p. 278
81. Peppas. N. A, Hilt. J. Z, Khademhosseini. A, Langer. R, *Adv. Mater.*, 2006, **18**, p. 1345
82. Elisseeff. J. H, Yamada. Y, Langer. R, Lewandrowski. K. U, *Marcel Dekker*, 2002, **1**, p. 1
83. Peppas. N, *Boca Raton*, 1987, **3**, p. 177

84. Brannon-Peppas. L, Harland. R. S, *Elsevier*, 1990, **1**, p. 45
85. Weber. L. M, Lopez. C. G, Anseth. K. S, *J. Biomed. Mater. Res.*, 2009, **90**, p. 720
86. Nuttelman. C. R, Tripodi. M. C, Anseth. K. S, *J. Biomed. Mater. Res.*, 2006, **76**, p. 183
87. Schoenmakers. R. G, van de Wetering. P, Elbert. D. L, Hubbell. J. A, *J. Control*, 2004, **95**, p. 291
88. Lee. Y, Chung. H. J, Yeo. S, Ahn. C. H, Lee. H, Messersmith. P. B, Park. T. G, *Soft Matt.*, 2010, **6**, p. 977
89. Wen. Z, Xing. J, Yang. C, Yuying. L, Jun. F, *J. Chem. Technol. Biotechnol.*, 2013, **88**, p. 327
90. Maolin. Z, Jun. L, Min. H, Hongfei. H, *Radiat. Phys. Chem.*, 2000, **58**, p. 397
91. Yang. L, Chu. J. S, Fix. F. A, *Int. J. Pharm.*, 2002, **235**, p. 1
92. Takashi. L, Hatsumi. T, Makoto. M, Takashi. I, Takehiko. G, Shuji. S, *J. Appl. Polym. Sci.*, 2007, **107**, p. 842
93. Ahmed. E. M, *J Adv. Res.*, 2015, **6**, p. 105
94. Maherani. B, Arab-Tehrany. E, Mozafari. M. R, Gaiani. C, Linder. M, *Curr. Nanosci.*, 2011, **7**, p. 436
95. Lee. H, McKeon. R. J, Bellamkonda. R. V, *Proc. Natl. Acad. Sci.*, 2010, **107**, p. 3340
96. Hoare. T. R, Kohane. D. S, *Polymer*, 2008, **49**, p. 1993
97. Jeong. B, Bae. Y. H, Lee. D. S, Kim. S. W, *Nature*, 1997, **388**, p. 860
98. Jeong. B, Choi. Y. K, Bae. Y. H, Zentner. G, Kim. S. W, *J. Cont. Rel.*, 1999, **62**, p. 109
99. Jeong. B, Bae. Y. H, Kim. S. W, *Macro*, 1999, **32**, p. 7064
100. Van Tomme. S. R, Storm. G, Hennink. W. E, *Int. J. Pharm.*, 2008, **355**, p. 1
101. Nguyen. K. T, West. J. L, *Biomaterials*, 2002, **23**, p. 4307
102. Scranton. A. B, Bowman. C. N, Peiffer. R. W, *Crit. Rev. Opt. Sci. Tech.*, 1996, **63**. P. 136
103. Elisseeff. J, Anseth. K, Sims. D, McIntosh. W, Randolph. M, Yaremchuk. M, Langer. R, *Plast. Reconstr. Surg.*, 1999, **104**, p. 1014
104. Martens. P. J, Bryant. S J, Anseth. K. S, *Biomacromolecules*, 2003, **4**, p. 283
105. Burdick. J. A, Anseth. K. S, *Biomaterials*, 2002, **23**, p. 4315
106. Bryant. S. J, Anseth. K. S, *J. Biomed. Mater. Res.*, 2003, **64**, p. 70
107. Elisseeff. J, McIntosh. W, Anseth. K, Riley. S, Ragan. P, Langer. R, *J. Biomed. Mater. Res.*, 2000, **51**, p. 164
108. Sawhney. A. S, Pathak. C. P, Hubbell. J. A, *Macromolecules*, 1993, **26**, p. 581
109. Burdick. J. A, Anseth. K. S, *Biomaterial*, 2002, **23**, p. 4315
110. Matsuda. T, Kondo. A, Makino. K, Akutsu. T, *ASAIO. Trans*, 1989, **35**, p. 67
111. Shibataa. H, Heoa. Y. J, Okitsua. T, Matsunagaa. Y, Kawanishia. T, Takeuchia. S, *PNAS*, 2010, **107**, p. 17894
112. Barry. A. P, Barry. N. P. E, *Polym. Chem.*, 2014, **5**, p. 3291
113. Alexandridis. P, Holzwarth. J. F, Hatton. T. A, *Macromolecules*, 1994, **27**, p. 2414
114. Alexandridis. P, Holzwarth. J. F, *Curr. Opin. Coll. Int. Sci.*, 2000, **5**, p. 312

115. Thurn. T, Couderc. S, Sidhu. J, Bloor. D, Penfold. J, Holzwarth. J, Wyn-Jones. E, *Langmuir*, 2002, **18**, p. 9267
116. Yang. L, Alexandridis. P, Steytler. D, Kositz. M, Holzwarth. J, *Langmuir*, 2000, **16**, p. 8555
117. Kabanov. A, Lemieux. P, Vinogradov. S, Alakhov. V, *Adv. Dru. Del. Rev.*, 2002a, **54**, p. 223
118. Singh. V, Khullar. P, Dave. P. N, Kaur. N, *Int. J. Ind. Chem.*, 2013b, **4**, p. 1
119. Cau. F, Lacelle. S, *Macromolecules*, 1996, **29**, p. 170
120. Nagarajan. R, *Coll. Surf. B: Bioint.*, 1999, **16**, p. 55
121. Rapoport. N, *Coll. Surf. B: Bioint*, 1999, **16**, p. 93
122. Alakhov. V. Y, Kabanov. A. V, *Exp. Opin. Invest. Drugs*, 1998, **7**, p. 1453
123. Batrakova. E. V, *Br. J. Cancer*, 1996, **74**, p. 1545
124. Wang. P. L, Johnston. T. P, *Int. J. Pharm.*, 1993, **96**, p. 41
125. Wang. P. L, Johnston. T. P, *J. Parenter. Sci. Technol.*, 1993, **47**, p. 183
126. Larson. N, Ghandehari. H, *Chem. Of Mat.*, 2012, **24**, p. 840
127. Kabanov. A, Lemieux. P, Vinogradov. S, Alakhov. V, *Adv. Drug Del. Rev.*, 2002b, **54**, p. 223
128. Huntsman Corp.,  
[http://www.huntsman.com/portal/page/portal/performance\\_products/Media%20Library/global/files/jef\\_famine\\_polyetheramines.pdf](http://www.huntsman.com/portal/page/portal/performance_products/Media%20Library/global/files/jef_famine_polyetheramines.pdf), 2012, Accessed: 09/08/2017
129. Hochhauser. D, Tobias. J. S, *Canc. Manag.*, 2014, **7**, p. 119
130. McKay. G. A, Walters. M. R, *Lec. Not. Clin. Phar. Ther.*, 2013, **9**, p. 1
131. Granberg. R. A, Rasmuson. A. C, *J. Chem. Eng. Data*, **1999**, **44**, p. **1391**
132. Drugs.com, <https://www.drugs.com/sfx/paracetamol-side-effects.html>, 2017, Accessed: 11/08/2017
133. Sepia Pharmacokinetics, <https://sepia.unil.ch/pharmacology/index.php?id=100>, 2009, Accessed: 14/08/2017
134. Sigma Aldrich, <http://www.sigmaaldrich.com/catalog/product/sial/a3035?lang=en&region=US>, 2017, Accessed: 11/08/2017
135. Harris. R. E, Beebe-Donk. J, Doss. H, Burr Doss. D, *Onc. Rep.*, 2005, **13**, p. 559
136. National Center for Biotechnology Information,  
<https://pubchem.ncbi.nlm.nih.gov/compound/ibuprofen#section=Top> 2017, Accessed: 14/08/2017
137. O'Neil. M. J, *Enc. Chem. Drug. Bio.*, 2001, **13**, p. 876
138. Nayak. A, Jain. A, *Scient. Pharm.*, 2011, **79**, p. 359
139. Sigma Aldrich, <http://www.sigmaaldrich.com/catalog/product/sigma/i4883?lang=en&region=GB>, 2017, Accessed: 14/08/2017

140. Cao. L, Wang. X, Meziani. M. J, Lu. F, Wang. H, Luo. P. G, Lin. Y, Harruff. B. A, Veca. L. M, Murray. D, Xie. S. Y, Sun. Y. P, *J. Am. Chem. Soc.*, 2007, **129**, p. 11318
141. Pan. D, Zhang. J, Li. Z, Wu. C, Yan. X, Wu. M, *Chem. Comm.*, 2010, **46**, p. 3681
142. Ray. S. C, Saha. A, Jana. N. R, Sarkar. R. J, *Phys. Chem. C.*, 2009, **113**, p. 18549
143. Buorlinos. A. B, Stassinopoulos. A, Anglos. D, Zboril. R, Karakassides. M, Giannelis. E. P, *Small*, 2008, **4**, p. 455
144. Buorlinos. A. B, Stassinopoulos. A, Anglos. D, Zboril. R, Georgakilas. V, Giannelis. E. P, *Chem. Mater.*, 2008, **20**, p. 4539
145. Dong. Y, Shao. J, Chen. C, Li. H, Wang. R, Chi. Y, Lin. X, Chen. G, *Carbon*, 2012a, **50**, p. 4738
146. Li. H, He. X, Liu. Y, Yu. H, Kang. Z, Lee. S, *Mat. Res. Bull.*, 2011, **46**, p. 147
147. Jiang. K, Sun. S, Zhang. L, Lu. Y, Wu. A, Cai. C, Lin. H, *Ang. Chem. Int. Ed.*, 2015, **54**, p. 5360
148. Wang. F, Xie. Z, Zhang. H, Liu. C, Zhang. Y, *Adv. Func. Mat.*, 2011, **21**, p. 1027
149. Wang. Y, Baker. S, Pro. Q. Diss. Pub., 2013, **1**, p. 23
150. Liu. Z, Liu. D, Wang. L, Zhang. J, Zhang. N, *Int. J. Mol. Sci.*, 2011, **12**, p. 1684
151. Han. L, Guo. J, Zhang. L, Wang. Q, Fang. X, *Pharm. Sini.*, 2006, **27**, p. 747
152. Jeong. B, Bae. Y. H, Kim. S. W, *J. Cont. Rel.*, 2000, **63**, p. 155